# Defense Intelligence Reference Document

[redacted]

*Acquisition Threat Support*

6 April 2010

ICOD: 1 December 2009

DIA-08-1004-006

# Metamaterials for Aerospace Applications

# Metamaterials for Aerospace Applications

**Prepared by:**

(b)(3):10 USC 424

**Defense Intelligence Agency**

**Author:**

(b)(6)

**Administrative Note**



This product is one in a series of advanced technology reports produced in FY 2009 under the Defense Intelligence Agency, (b)(3):10 USC 424 Advanced Aerospace Weapon System Applications (AAWSA) Program. Comments or questions pertaining to this document should be addressed to (b)(3):10 USC 424;(b)(6)., AAWSA Program Manager, Defense Intelligence Agency, ATTN: (b)(3):10 USC 424 Bldg 6000, Washington, DC 20340-5100.

## Contents



## Figures

## Definition of Metamaterials

A metamaterial is defined as an artificial medium whose properties (mechanical, optical, magnetic, or other) cannot be found in naturally-occurring materials. The emphasis of this study will be on electromagnetic and optical metamaterials. Such metamaterials can exhibit rather extreme properties, such as negative refractive index, which implies that both electric permittivity and magnetic permeability must be negative ($\varepsilon < 0$, $\mu < 0$) (Reference 1). Such metamaterials used to be called "left-handed" because of the unusual phase relationship between the electric and magnetic fields. Specifically, in most (positive index, including vacuum) media one uses the right-hand rule to define the relationship between electric field ($\vec{E}$) magnetic field ($\vec{H}$), and the propagation wavenumber ($\vec{k}$). The physical basis of the right-hand rule is that the direction of energy propagation defined by the Poynting vector $\vec{S} = c\vec{E} \times \vec{H} / 4\pi$ and the direction of the phase velocity (defined by the wavenumber $\vec{k}$) must coincide. That does not hold true for negative index metamaterials where the two directions are opposite, therefore, the left-handed relationship must hold for the three vectors. Nevertheless, the "left-handed" designation did not withstand the test of time because it was causing confusion and creating irrelevant allusions to helical (a.k.a. chiral) structures. Although chiral structures can indeed exhibit negative index behavior (Reference 2), chirality is not necessary.

A typical metamaterial consists of resonant elements such as Split Ring Resonators (SRR). An example of an SRR is shown in Figure 1. The main function of the SRR is to enable strong magnetic response of the structure. A simple empirical formula exists for the magnetic permeability of a metamaterial comprised of the SRRs:

$$\mu = 1 - \frac{F\omega_M^2}{\omega^2 - \omega_M^2} < 0, \qquad (1)$$

where $\omega_M$ is the resonant frequency of the SRR, and $F$ is proportional to the volume filling factor of SRRs. It is noteworthy that SRRs are designed in such a way that it has a large capacitance. As the result, the resonant frequency of an SRR is small, (that is, the SRR-containing cell is very sub-wavelength). In the example shown in Figure 1 (taken from Reference 6), the unit cell operated at $\omega/2\pi$ = 10 GHz is $\lambda/10$. In fact, the sub-wavelength size of the metamaterial is what distinguishes them from their close cousins: photonic crystals. By properly designing magnetic SRRs, it is possible to achieve any value of $\mu$ for any given frequency. Special challenges exist for optical structures, though, as will be explained below.

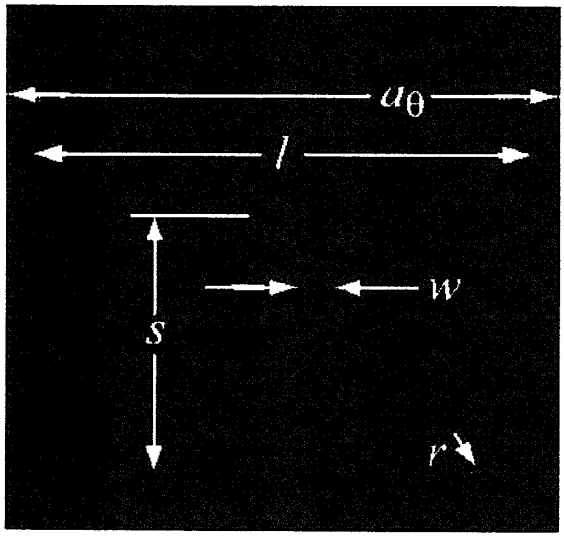


| cyl. | $r$ | $s$ | $\mu_r$ |
|---|---|---|---|
| 1 | 0.260 | 1.654 | 0.003 |
| 2 | 0.254 | 1.677 | 0.023 |
| 3 | 0.245 | 1.718 | 0.052 |
| 4 | 0.230 | 1.771 | 0.085 |
| 5 | 0.208 | 1.825 | 0.120 |
| 6 | 0.190 | 1.886 | 0.154 |
| 7 | 0.173 | 1.951 | 0.188 |
| 8 | 0.148 | 2.027 | 0.220 |
| 9 | 0.129 | 2.110 | 0.250 |
| 10 | 0.116 | 2.199 | 0.279 |

**Figure 1. Example of a Metamaterial Component: The Magnetic Split Ring Resonator (SRR) Design.** The in-plane lattice parameters are $a_y = a_z = 10/3$ mm. The ring is square, with edge length l =3 mm and tracewidth w = 0.2 mm. The substrate is 381 μm-thick Duroid 5870 ($\varepsilon = 2.33$, $t_d = 0.0012$ at 10 GHz, where $t_d$ is the loss tangent). The Cu film, from which the SRRs are patterned, is 17 μm thick. The parameters r and s are given in the table together with the associated value of $\mu_r$. (Reference 6)

Electric properties of metamaterials can be similarly controlled. An example of a planar electrically-active metamaterial is shown in Figure 2.

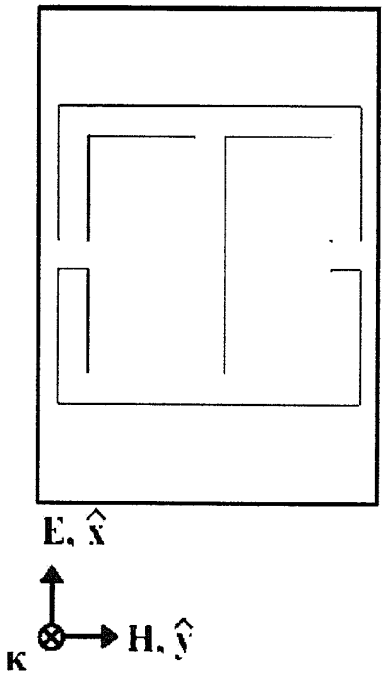


**Figure 2. Example of Another Metamaterial Component: Electric Ring Resonator (ERR).** This component provides tunable resonant electric response to the incident electromagnetic field, and can be utilized for engineering the frequency-dependent dielectric permittivity $\varepsilon(\omega)$. Possible application: *THz* and microwave absorbers. (Reference 7)

The electric response of such (or similar) metamaterial is given by

$$\varepsilon(\omega) = 1 - \frac{\omega_p^2}{\omega^2 - \omega_R^2 + i\omega\gamma} \tag{2}$$

where $\omega_R$ is the resonant frequency and $\gamma$ is the loss coefficient.

Negative index metamaterials are by no means the only potentially useful metamedia. Several new concepts such as Indefinite Permittivity Metamaterials (IPM) (References 3, 4) and Epsilon-Near-Zero (ENZ) metamaterials (Reference 5) have recently emerged and found some exciting applications that will be reviewed below. IPMs can be used as ultra-compact spatial filters (both high-pass and low-pass) whereas ENR metamaterials can be used for making sub-wavelength waveguides capable of coupling close to 100 percent of the incident radiation (Reference 8), as well as directing it around tight bends with negligible bending losses. Yet another class of planar metamaterials, complementary metamaterials (CMMs), has recently emerged (Reference 7). Instead of using metallic structures deposited on a substrate (left panel of Figure 3), CMMs consist of slits in the continuous metal screen (right panel of Figure 3). The shape of the slits coincides with that of the materials themselves. Such complementary metamaterials have been recently used for making epsilon-near zero waveguides (Reference 8).

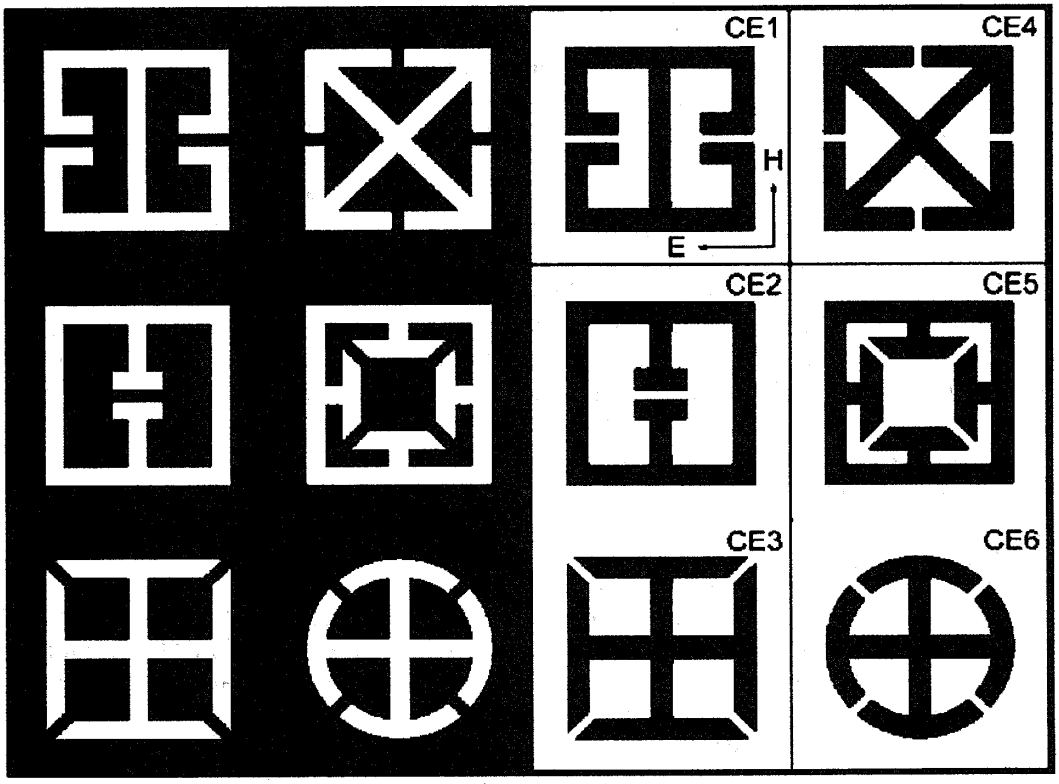


**Figure 3. Geometry of Original Planar Metamaterial Unit Cells (OE1-OE6) and Their Complements (CE1-CE6).** The polarization of normally incident electromagnetic radiation is configured as shown in OE1 and CE1 for the original and complementary metamaterials, respectively. (Reference 9)

In general, metamaterials offer a new way of designing electromagnetic structures with arbitrary values of permittivity/permeability tensors, as well as other parameters (such as bi-anisotropy coefficient). In many instances, metamaterials enable us to considerably minimize sizes of resonators, transmission lines, and so forth. Such miniaturization is possible due to the resonant nature of the individual unit cells. Specifically, the structures shown in Figure 3 have high capacitance; therefore, their individual sizes are very sub-wavelength. That enables arrangement within sub-wavelength units that can be densely packed and result in strongly miniaturized components. It is this miniaturization that makes metamaterials interesting for aerospace application where small weight and size are essential.

While the most spectacular progress in the field of electromagnetic metamaterials has so far occurred in the microwave range, it is the optical (visible, infrared, mid-infrared) spectral regions that hold most promise for revolutionary applications. Electromagnetic metamaterials have a tremendous potential for revolutionizing propagation, storage, and conversion of electromagnetic waves across the entire Electromagnetic Spectrum. In our opinion, the most exciting applications that are relevant for aerospace applications include energy harvesting, developing novel optical devices with unusual yet practically important capabilities (for example, non-reciprocal devices), enhancing the efficiency of nonlinear optical devices, developing novel imaging modalities capable of breaking the diffraction limit (for example, super-lenses, hyper-lenses, far field super-lenses), and developing novel lithographic techniques.

Optical metamaterials are still a very new area. Just a handful of experimental demonstrations of multi-layer (truly bulk) optical metamaterials exist at the moment. Among the most recent ones are (a) demonstration of the negative index optical metamaterial at the telecommunications wavelength (Reference 10) that used the so-called fishnet structure shaped as a prism for demonstrating Snell's Law, and (b) demonstration of the Indefinite Permittivity Material (IPM) and *negative refraction* (which, in the context of anisotropic metamaterials, is not the same as *negative refractive index*) in the mid-infrared part of the spectrum (Reference 11). These structures have the distinction of being multi-layer (or bulk). Most previous examples of optical metamaterials have dealt with single or double-layer substances which cannot be, strictly speaking, characterized as metamaterials. The difficulty in obtaining strong magnetic activity in optical metamaterials has been explained in several recent reviews (References 12, 13). In a nutshell, the issue is that the magnetic moment of most structures (including atomic systems) is very small, much smaller than the electric moment. Therefore, it is difficult to observe any optical effects that can be clearly assigned to magnetic activity. This is especially true for the structures that are much smaller than one wavelength. Exceptions, such as artificially constructed split rings, are possible. However, such structures cannot be operated at very high frequency because of the excitation of electrostatic resonances (Reference 12). In other words, when the resonant frequency is too high (or the dielectric permittivity of a metal is not sufficiently large), electrostatic resonances disrupt magnetic activity. More specifically, the energy inside and in the vicinity of a metamaterial element (for example, Split Ring Resonator) becomes predominantly electrostatic, (that is, in the form of the kinetic energy of oscillating electrons). The recently described multi-layer fishnet (Reference 10) is not an exception: its unit cell (that is, the lateral period) is only one-half of the operating wavelength.

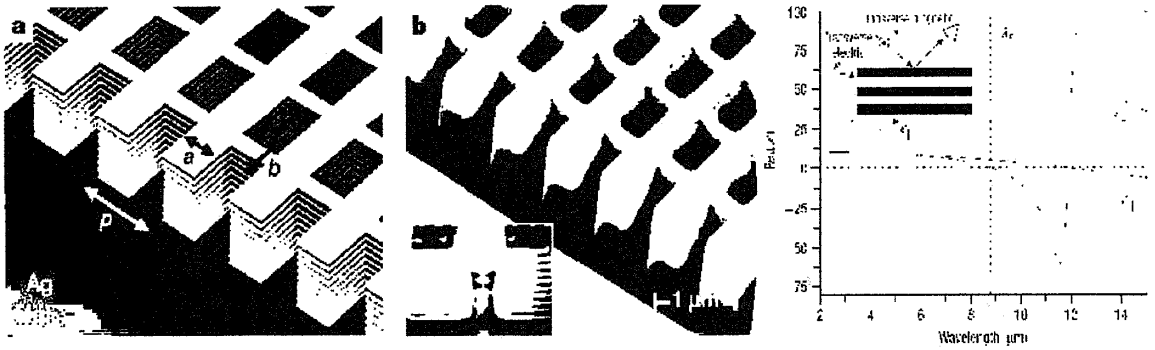


**Figure 4. Recent Optical Metamaterials for Telecommunication Wavelength λ = 1.5 μm (Left and Middle) and Mid-Infrared IPM.** The multi-layer fishnet is made of silver films separated by a dielectric spacer. A focused ion beam was used to produce the prism-shaped fishnet. The IPM was obtained by depositing interleaved 80 nm layers of $In_{0.53}Ga_{0.47}As$ and $Al_{0.48}In_{0.52}As$. The layers, approximately 8.1 μm thick, grown by molecular beam epitaxy on lattice-matched InP substrates. The InGaAs layers were uniformly doped to create different values of permittivity in alternating layers. (Reference 10 and 11)

That is not to say that there is not ongoing theoretical and experimental work on designing optical metamaterials for practical applications. The author's research group at UT- Austin, has designed the first Plasmonic Negative Index Metamaterials (P-NIM) super-lens (Reference 14), developed novel techniques for analyzing optical properties of plasmonic nanostructures, (including band-structure calculations of periodic nanostructures) (Reference 15) and quasi-static calculations of plasmonic resonances (Reference 16). The UT-Austin group has also designed a number of unique sub-wavelength P-NIMs in the optical part of the spectrum (References 14, 17, 18), and has recently published a review of optical P-NIMs (Reference 12). The group has also contributed to developing and experimentally implementing the concept of the "perfect lens" (Reference 19) based on plasmonic/polaritonic materials. A perfect lens enables imaging of sub-wavelength objects in the infrared part of the spectrum, including objects buried under the surface. Also developed is a Wide-Angle "Perfect" Absorber of Mid-Infrared Radiation (WAPAMIR) (Reference 20) based on the negative index metamaterial whose impedance is perfectly matched to vacuum.

Below is a concise summary of various topics/applications that are especially suitable for the aerospace industry. This study concentrates on the facility of metamaterials to miniaturize various optical and microwave components. Metamaterials can also be used for imaging very small (sub-wavelength) objects without resorting to costly and space-consuming near-field scanning optical microscopy. Also described are the ongoing efforts in the field to make extremely compact metamaterials-based lasers. Smaller lasers mean smaller weight and more room for other diagnostic devices and useful payload within the confines of a space vehicle. Applications of metamaterials to photon harvesting is especially fitting for advanced aerospace platforms because of the necessity to collect electromagnetic energy for battery recharging, diagnostic spectroscopy, and other vital functions of a space vehicle.

- **Complementary Metamaterials for Energy Harvesting.** Development of ultra-thin photovoltaic and thermo-photovoltaic cells is hampered by weak photon absorption in semiconductors. Metamaterials can modify absorption making it wavelength-selective (tunable), highly efficient, and, if desired, wide-angle. Recently a way has been found for creating quarter-wavelength resonators backed by leaky mirrors made out of CMMs.

- **Far Field Super-Lens Based on the Interferometry of Sub-Diffraction Waves.** Sub-diffraction imaging has long been considered to be possible only using near-field microscopes. Those are fairly complex, slow-scanning, and large devices that are not appropriate for advanced aerospace platforms. Metamaterials enable new imaging modalities: super-lenses, hyper-lenses, and far-field super-lenses. In addition to a survey of the existing scientific literature, novel ideas on developing a new interferometric Far-field Super-Lens (FSL) based on the multi-beam multi-detector technique utilizing materials with Indefinite Permitivity Tensor are presented. Fabrication of such Indefinite Permittivity Materials (IPMs) for the mid-infrared part of the spectrum is achieved and demonstrates the capabilities of transmitting electromagnetic waves with the spatial period much smaller than the vacuum wavelength of light. Interference between sub-diffraction waves enables disentangling multiple diffractive orders and extracting their amplitudes.

- **Nonlinear Non-Reciprocal Chiral Metamaterials: Developing Novel Optical Isolators and "One-Way" Microwave Mirrors.** These developments are motivated by the need to construct one-way "light diodes" for compact optical isolators. Presently there are two approaches to optical isolation: the most common using magnetic fields, and the less developed based on using nonlinearities. A different approach relies on the phenomenon of adiabatic mode conversion in nonlinear chiral metamaterials. Preliminary theoretical results for a simple chiral fiber with a variable twist period (pitch) that enables full transmission of a tightly confined core mode in the forward direction and full mode-conversion of the core mode into a cladding mode for the backwards propagation is obtained.

- **Slowing Down Light and Miniaturizing Optical Components Using the Phenomenon of Electromagnetically Induced Transparency in Metamaterials.** The speed of light places a natural limit on the size of optical/microwave components. Metamaterials offer an exciting opportunity to slow down light. This has two major implications: (a) light can be stored/manipulated in smaller volumes, and (b) nonlinear effects are strongly enhanced by the resulting energy compression.

## Applications to Sub-Diffraction Imaging: Super-Lens and Hyper-Lens

The super-lens is one of the earliest applications of metamaterials (Reference 21), and its principle is shown is Figure 5. Without the super-lens, all information about sub-diffraction (or sub-wavelengths, which is equivalent) features of the periodic object would have been lost. The reason for the information loss is evanescent decay of the large spatial wavenumbers. The only method of accessing/measuring these features would be to scan the object using a near field scanning optical microscope. By inserting a super-lens between the object and the imaging plane, evanescent waves may be amplified and the image transferred forward. Unfortunately, this approach by itself does not remove the need for a near-field scanning device; the image that is recreated in the imaging plane is still sub-wavelength, and needs to be read out.

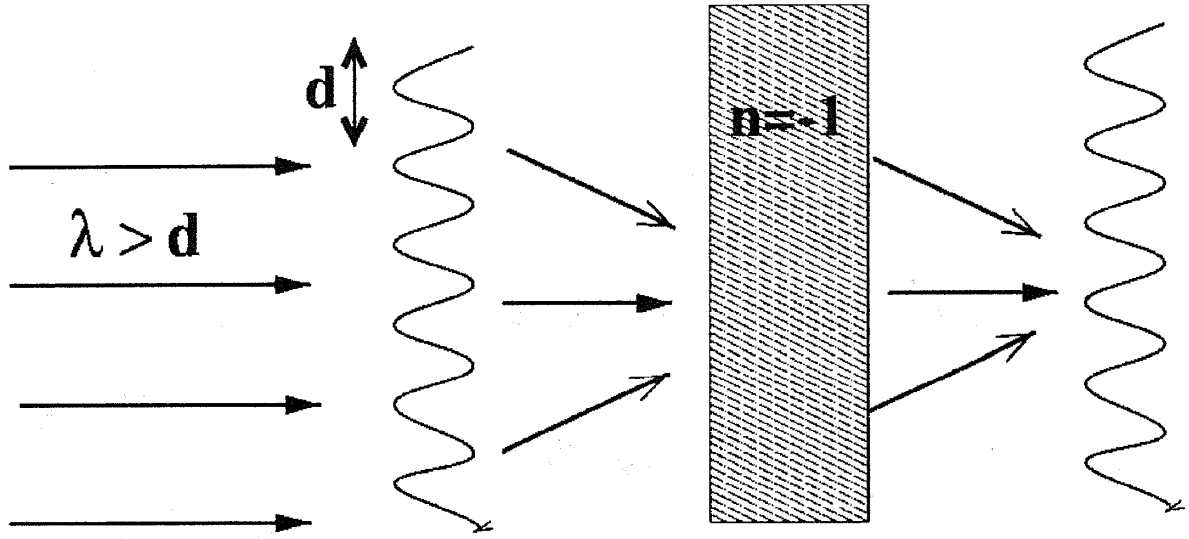


**Figure 5. Schematic of the Super-Lens with n=-1 Refractive Index Corresponding to (ε = -1, μ = -1) Surrounded By Vacuum.** Super-lens' presence enables imaging sub-diffraction objects such as the periodic grating shown here.

There are, however, interesting circumstances when it is very important to transport the image towards the scanning device. One such special circumstance is spatially-resolved spectroscopy of small (for example, cellular) structures. One can envision space expeditions to other planets that could, potentially, result in finding some evidence of primitive cellular-level life. It would then be highly desirable to examine the structure of the living cell in its natural environment. In all likelihood, that environment would be liquid. Therefore, it would be very desirable to examine the cell without actually touching it with a tip of a near-field optical microscope. Thus, the sub-surface imaging of a small object which is buried underneath a liquid layer would be necessary. No such experiments have so far been conducted. However, several years ago there was an experiment demonstrating imaging of sub-diffraction objects buried under the layer of silicon dioxide.

The schematic and experimental results from the experiment (Reference 19) are shown in Figure 6. In this experiment the sub-wavelength objects were simple holes that were milled in the metal using an FIB. They were buried underneath the super-lens consisting of SiC (negative epsilon material for mid-infrared frequencies) and silicon dioxide (positive epsilon material). Note that this configuration (materials with $\varepsilon_1 > 0$ and $\varepsilon_2 \approx -\varepsilon_1 < 0$ joined together: sandwiched or positioned next to each other) is typical for a near-field super-lens. The difference between the near-field super-lens shown in Figure 6 and the "ideal" super-lens shown in Figure 5 is that the ideal also requires a material with a negative value of magnetic permeability.

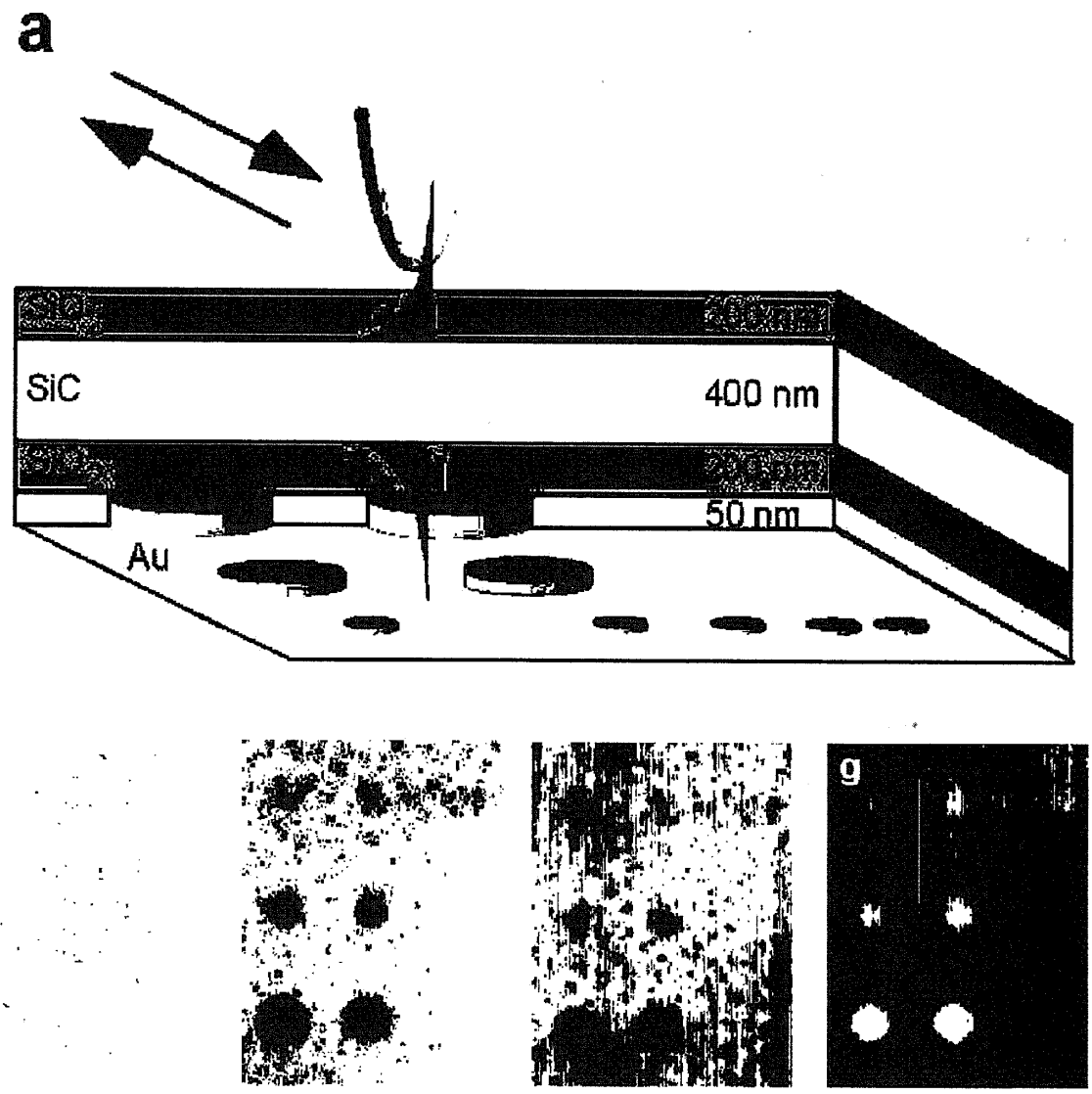


**Figure 6. Schematic of the SiC-Based Super-Lens Which is Imaging Sub-Wavelength Holes Buried Under the $SiO_2$ Layer.** The imaged objects are λ/20 holes milled in gold using FIB. The scattered signal is picked up by the tip of an NSOM and directed towards the IR detector. Depending on the imaging wavelength, either amplitude (e) or the phase (f,g) of the signal are prominent.

As the laser beam scatters off the sub-wavelength holes, its electric field is picked up by the tip of a Near-Field Scattering Optical Microscope (NSOM) and re-scattered into the far-field. There it is interfered with the reference pulse and picked up by an infrared detector. Note that this interferometric technique enables one to extract both the phase and amplitude of the field, as shown in Figure 6. This significantly broadens the spectral range over which the super-lens yields meaningful information. For example, the amplitude contrast is highest at $\lambda = 10.85$ μm shown in panel (e) while the phase contrasts are the highest at $\lambda = 11.03$ μm and $\lambda = 10.65$ μm.

Despite the convenience of the near-field super-lens, (that is, its ability to transport the image) it still requires an NSOM to read out the image. Within the confines of an advanced aerospace platform such device (with its necessary auxiliaries) may not fit. Therefore, one has to consider alternative metamaterials-based ideas for sub-diffraction imaging. One such idea, the hyper-lens, has been proposed recently by two groups (References 22-24), and already experimentally tested by another group (Reference 25). The principle of the hyper-lens is very simple: to use an indefinite permittivity medium (sometimes referred to as the hyperbolic medium because the relationship between the propagation wavenumbers and the frequency, also known as the constant frequency contour, has a hyperbolic nature) in a tapered format. Several conceptual implementations such as the spoke-like structure and the cylindrical multi-layer structure (see Figure 7, left panel) have been suggested. The hyper-lens works on two principles: (a) indefinite permittivity materials (of which the super-lens is one example) are capable of propagating sub-diffraction waves, and (b) the expanding nature of the hyper-lens can magnify images to the $\lambda/2$ size, at which point they become observable in a conventional microscope. One recent experimental implementation of the hyper-lens in UV is shown in the right panel of Figure 7. The hyper-lens is made of 16 layers of $Ag/Al_2O_3$. This specific hyper-lens was used for imaging a line pair object with line width of 35 nm and spacing of 150 nm and was operated at $\lambda$ =400 nm. The magnified image (350 nm spacing) can be clearly resolved with an optical microscope [numerical aperture (NA) = 1.4], thus demonstrating magnification and projection of a sub-diffraction-limited image into the far field.

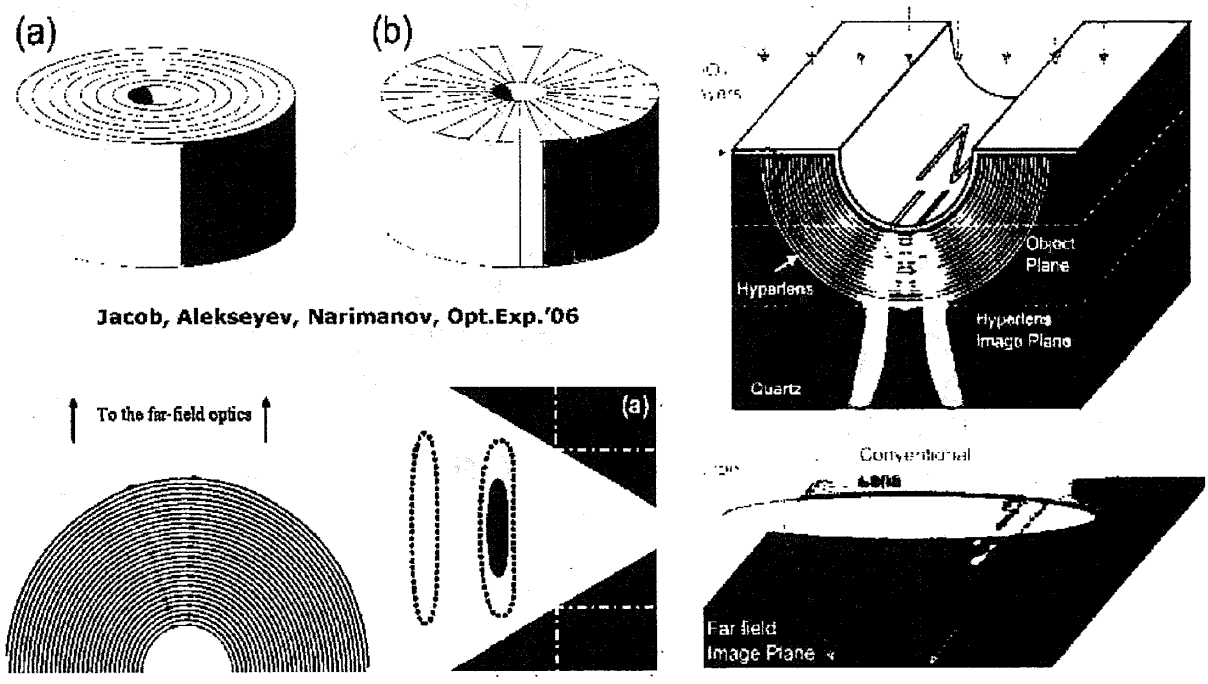


**Figure 7. Theoretical Concepts (left panel) and Experimental Implementation (right panel) of an Optical Hyper-lens Capable of Magnifying Sub-Diffraction Objects to Observable (larger than $\lambda/2$) Size**

Note that the hyper-lens concept does not require employing a bulky near-field scanning optical microscope. However, the practical implementation of the hyper-lens is by no means simple. The original implementation required depositing the sample on the curved surface of the hyper-lens. A more practical implementation of the super-lens has been theoretically proposed by another group (Reference 26). The concept is shown in Figure 8. The hyper-lens involves an array of thin metallic wires converging towards the tip. As is demonstrated, a dense array of metal wires separated by much less than the wavelength constitutes a metamaterial with the indefinite permittivity tensor. Specifically, the tensor component along the wires is given by:

$$\varepsilon_{zz} = 1 - \omega_p^2/(\omega^2 - k_z^2 c^2) \text{ and } \varepsilon_{\perp} = 1, \tag{3}$$

where the z component is along the wires and perpendicular direction is normal to the wires. Because the only propagating waves are the TEM waves satisfying the $\omega^2 = k_z^2 c^2$ dispersion relation, this meta-medium is strongly anisotropic and supports sub-wavelength waves which perform imaging. The spatial resolution is given by the spacing between wires. Figure 8 (right panel) shows the magnified image of a small ($\lambda/25$) object placed at the tip of the hyper-lens. The magnification factor is 5x.

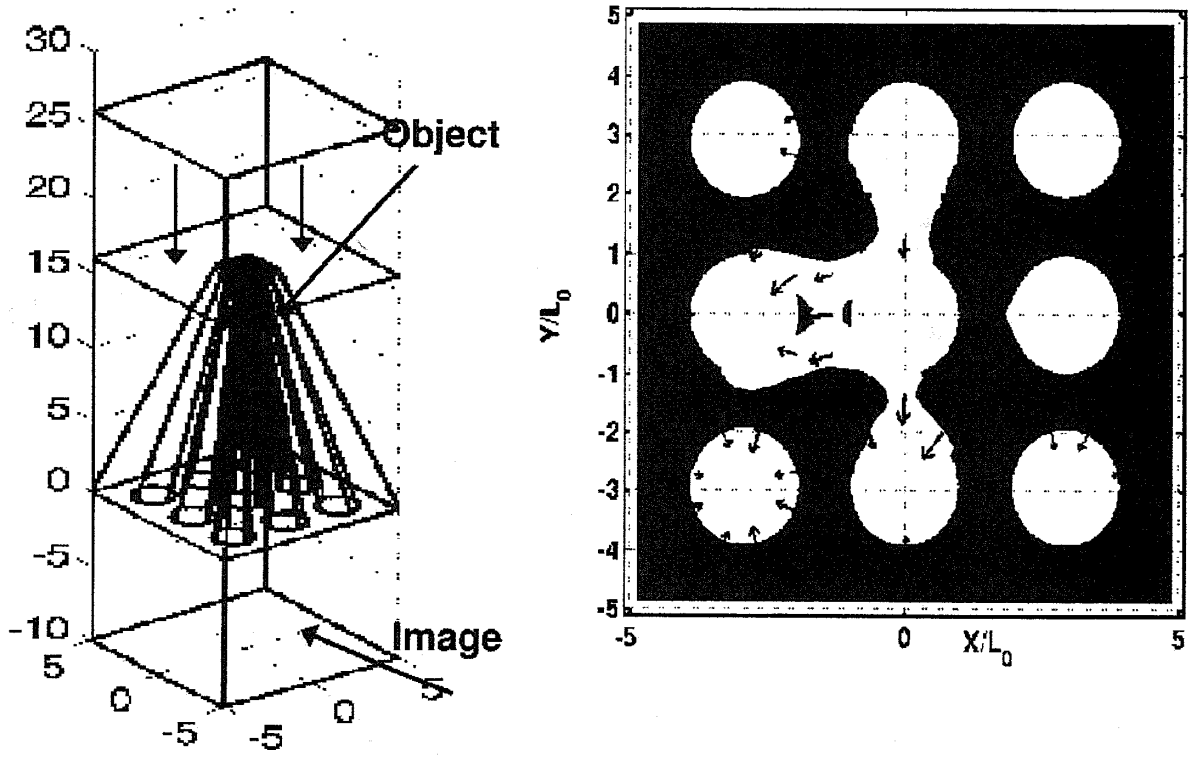


**Figure 8. Hyper-Lens Based on a Converging Array of Metal Wires.** A small object can be placed at the tip, illuminated from the top, and magnified by the expanding array of wires. Left panel: schematic. Right panel: λ/25 object magnified by a factor 5x by the expanding hyper-lens. This hyper-lens can operate at mid-IR frequencies. (Reference 26)

Another concept for sub-wavelength imaging employing metamaterials is the so-called Far-Field Super-Lens (FSL). The concept is pioneered in Reference 27. The idea is

described in Figure 9. A sub-wavelength object (for example, two slits) is located at the bottom of a multi-layer super-lens. Another sub-wavelength grating is deposited on top of the super-lens. Because the super-lens (and for that matter, any indefinite permittivity material) is capable of propagating sub-diffraction waves, the electromagnetic perturbations created by the object are propagated through the super-lens upwards, until they encounter the sub-wavelength grating. At that point these sub-wavelength perturbations are diffracted on the image-releasing grating and converted into the far-field electromagnetic waves. Those far-field waves are collected by the objective of a microscope and observed through the eyepiece. The schematic is shown in Figure 9(a). Note that, again, there is no need for NSOM. The actual implementation of the FSL used the following object: a nanowire pair with 50 nm wide slit and 70 nm gap inscribed by focused ion beam on a 40 nm thick Cr film on the quartz substrate. Diffraction-limited image from a conventional optical microscope cannot resolve the two nanowires (NA = 1.4, $\lambda_0$ = 377 nm) as can be seen in Figure 9(c), but the FSL-equipped microscope can as shown in Figure 9(d).

Despite the success of this demonstration, there are serious issues involved in imaging sub-wavelength objects. Specifically it is pointed out in Reference 27 that multiple diffractive orders can become entangled, (that is, launched in the same direction into the far field). Disentangling these diffraction orders is very important. The payoff would be imaging of fully 2-D (flat) objects with a resolution smaller than the period of the image-releasing grating. More precisely, this ambiguity is illustrated by the right panel in Figure 10. If the sub-wavelength object is represented by the continuous spectrum (blue line), then the spectrum can be sampled within the discrete set of "zones" which are defined by the diffractive orders of the image-releasing grating. The width of each zone is $2\omega/c$, and they are labeled as 1st order, 2nd order, and so forth. Wave numbers belonging to the different zones can be diffracted onto the same far-field detector as explained in Figure 10. In order to disentangle the 1st and the 2nd zones, a single detector cannot provide sufficient information. It turns out that using two detectors (A and B) and two laser beams (Beam A and Beam B) provides additional information that is sufficient to disentangle the two zones. This additional information is obtained by comparing the intensity on the two detectors A and B. Another advantage of this imaging technique is that it is interferometric in nature. Therefore, even if the contribution of some of these spectral zones' orders is very weak, it can still be detected because of the high sensitivity of the interferometric techniques. What makes this interference special is that it involves sub-diffractive waves propagating through the indefinite permittivity metamaterial. Below some of the experiments conducted in the laboratory that demonstrate such interference are discussed.

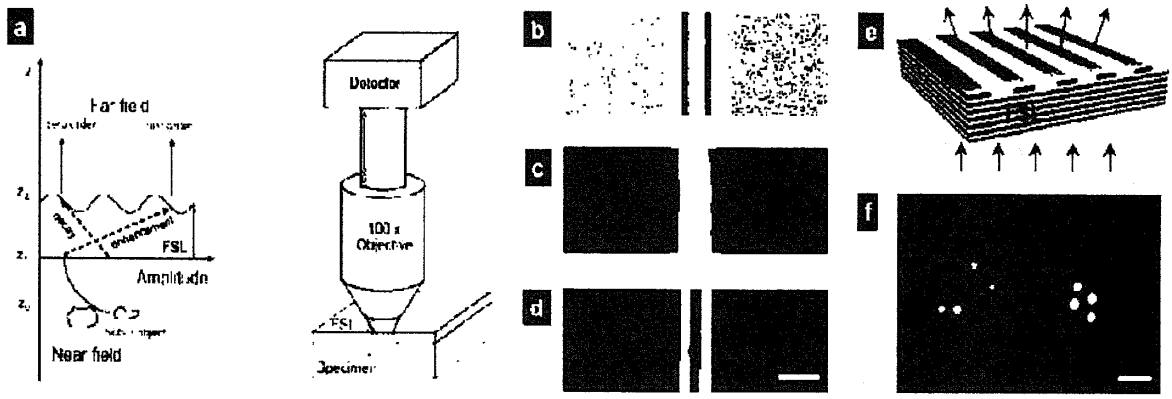


**Figure 9. FSL Based on an Indefinite Permittivity Metamaterial Placed Between the Object and the Image-Releasing Grating.** The grating releases into the far field sub-diffraction waves produced by light scattering off the object. The role of the metamaterial is to propagate sub-diffraction waves from object to grating. (Reference 27)

Ever since Merlin's invention (Reference 28) of the sub-diffraction near-field plate, it has become clear that the interference between sub-diffraction electromagnetic fields can result in the formation of a deeply sub-wavelength image. The near-field plate, however, is not an imaging device; its purpose is to create a well-defined image using an elaborate pre-fabricated sub-wavelength structure on the plate's surface. The goal for this study is to observe an a priori unknown sub-wavelength image using a near-field structure. In the past, successes (Reference 19) in retrieving images of sub-wavelength objects (such as λ/20 holes) using an NSOM for radiation detection are achieved. An NSOM is a near-field instrument, therefore, a much more desirable detection method would involve far-field detection. To advance this goal, and to develop a tool sometimes referred to as the FSL, we've initiated research on multi-beam multi-detector sub-wavelength holography illustrated in Figure 10.

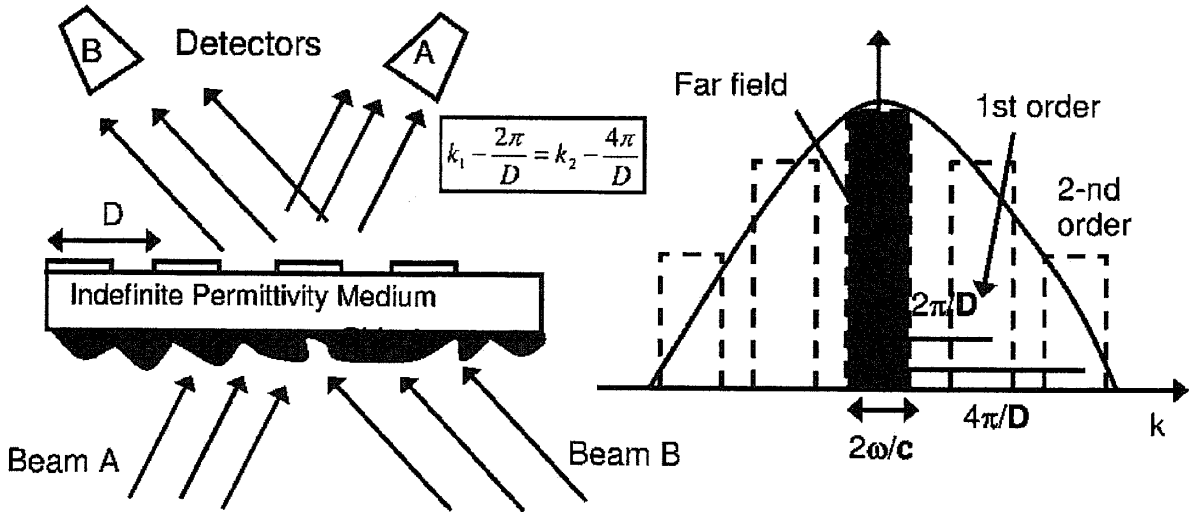


**Figure 10. Tomographic Multi-Beam Multi-Detector Holography of Sub-Wavelength Objects Using Indefinite Permittivity Medium (IPM).** Incident beam(s) scatter off the sub-λ object, propagate through the IPM, and then get re-scattered into the far field by the grating with the period D. The purpose of the multi-detector arrangement is to disentangle the $k_1$ and $k_2$ spatial wave numbers in the object's spectrum (shown in the left panel). Beams A and B are phase-shifted with respect to each other.

Our implementation of the FSL utilizes an IPM whose dielectric permittivity tensor is anisotropic and contains positive and negative components: $\varepsilon_{\perp} > 0, \varepsilon_{\parallel} < 0$, where parallel refers to the IPM/object interface. We have already fabricated such IPMs using $SiO_2$-SiC-$SiO_2$ multi-layer, and are investigating other approaches involving selectively-doped semiconductor multi-layers similar to the ones used by Gmachl's group at Princeton. $SiO_2$-SiC-$SiO_2$ multi-layers are produced in-house (with SiC films shipped by Professor Ferro from University of Lyons, France). The main function of the IPM is to propagate sub-diffraction waves ($k_{\parallel} > \omega/c$) with as little decay as possible. That happens because these sub-diffraction waves are no longer evanescent: $k_{\perp}^2 \approx -k_{\parallel}^2 \varepsilon_{\parallel} / \varepsilon_{\perp} > 0$. It is demonstrated experimentally that there exists a frequency range for which sub-diffraction waves propagate through the IPM with less attenuation than the radiation-zone waves ($k_{\parallel} < \omega/c$), see Figure 11.

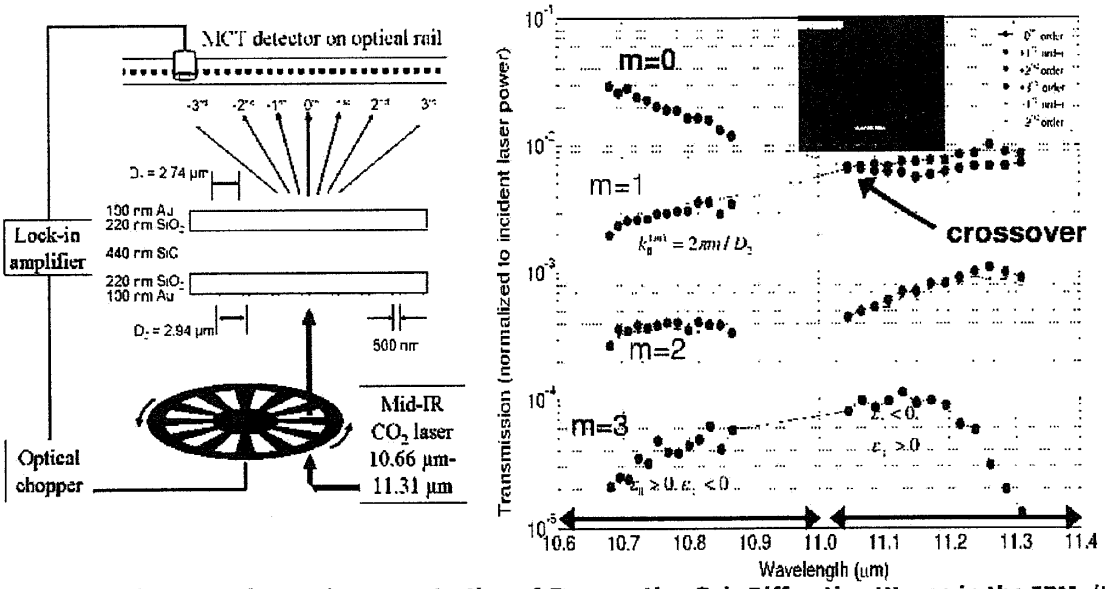


**Figure 11. First Experimental Demonstration of *Propagating* Sub-Diffraction Waves in the IPM.** (Left): Experimental setup demonstrating how sub-diffraction waves are launched into the IPM using FIB-fabricated sub-wavelength grating. Because the periods of the bottom ("launching") and top ("transforming") gratings are different, far-field observation of different harmonics of the bottom grating is enabled. (Right): Experimental results: the first sub-diffraction harmonic of the grating (green line) becomes stronger than the zeroth radiation-zone harmonic of the grating (blue line) in the region where $\varepsilon_{\perp} > 0, \varepsilon_{\parallel} < 0$.

Once sub-diffraction waves propagate through the IPM, they can diffract on the image-releasing grating (see Figure 10) and be radiated out into the far field. A detector array can be used to collect the signal and reconstruct the image. Unfortunately, different wave numbers $k_{\parallel}$ of the object are directed into the same detector and produce an ambiguity in extracting their respective amplitudes $A(k_{\parallel})$. This ambiguity is illustrated by Figure 10: wave numbers $k_1 = \Delta k + 2\pi/D$ and $k_2 = \Delta k + 4\pi/D$ are directed to the same far-field detector. Simply put, a single number (intensity of light with the wave number $\Delta k < \omega/c$ incident on the detector) is insufficient for determining two scattering

amplitudes ( $A(k_1)$ and $A(k_2)$ ). Therefore, a new concept has to be developed, and the multi-detector technique is such a concept.

The concept requires two detectors and two coherent laser beams. The two beams are formed using a beam-splitter and a variable delay line imparting a phase shift to the two beams (see the actual experimental photograph in Figure 13 where the beam-splitter BS and the Delay Line are shown). We have theoretically demonstrated that the intensity dependences of the two detector intensities $I_1(\psi)$ and $I_2(\psi)$ as a function of the phase delay $\psi$ provides enough information to recover both $A(k_1)$ and $A(k_2)$.

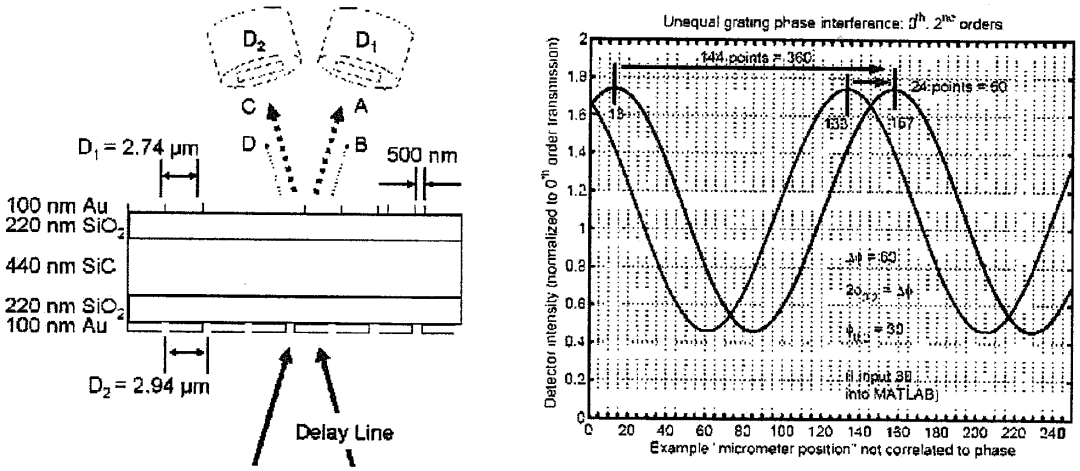


**Figure 12. (Left): Schematic for 2-Beams/2-Detectors Interferometric Measurement. (Right): Numerical Simulation:** intensity on the two detectors as a function of the phase delay between beams A and B produced by the interference between the zeroth and first diffractive orders of the bottom diffractive grating (numerical simulation). The second detector provides the necessary second data point which is necessary for separating the contributions of different diffractive orders.

Two sets of experiments demonstrating the feasibility of the concept are conducted. None of these experiments constitutes imaging per se. However, without demonstrating the two key milestones described below, proper imaging experiments cannot be attempted.

The first milestone involves demonstrating that IPM indeed supports propagating (non-evanescent) sub-diffraction waves. Figure 11 shows the experimental schematic (left panel) and experimental results. The bottom grating "imprints" its Fourier components (zeroth, first, second, third, and so forth) onto the incident laser pulse thereby generating electromagnetic waves that are launched into the SiC-based IPM. The zeroth harmonic is inside the radiation zone (that is, it is not sub-diffraction), while the first, second, and so forth sub-diffraction. These EM waves scatter off the top grating having a slightly different period and are released into the far field. Because the direction in which waves are released depend on the Fourier harmonic's number, we can experimentally separate and measure them. Clearly, the relative magnitudes of these diffractive orders dramatically vary as a function of the laser wavelength. For example, the zeroth diffraction order clearly dominates in the $\varepsilon_\perp < 0, \varepsilon_\parallel > 0$ frequency range. However, in the $\varepsilon_\perp > 0, \varepsilon_\parallel < 0$ frequency range the first diffractive order becomes larger

than the zeroth one. This confirms the recently predicted effect that for IPMs one can indeed observe a very counterintuitive effect: sub-diffraction waves can indeed propagate with less loss than the diffraction-limited ones.

The second milestone involves demonstrating the possibility of observing the interference of sub-diffraction electromagnetic waves inside the IPM using the two-beam/two-detector technique. Figure 10 demonstrates this interference pattern which reveals the phase advance of the sub-diffraction waves inside the IPM. While we have so far demonstrated the interference between the first Fourier component of the grating (sub-diffraction) and the zeroth Fourier component, we see the possibility of interfering even more sub-diffraction waves (2nd and 3rd).

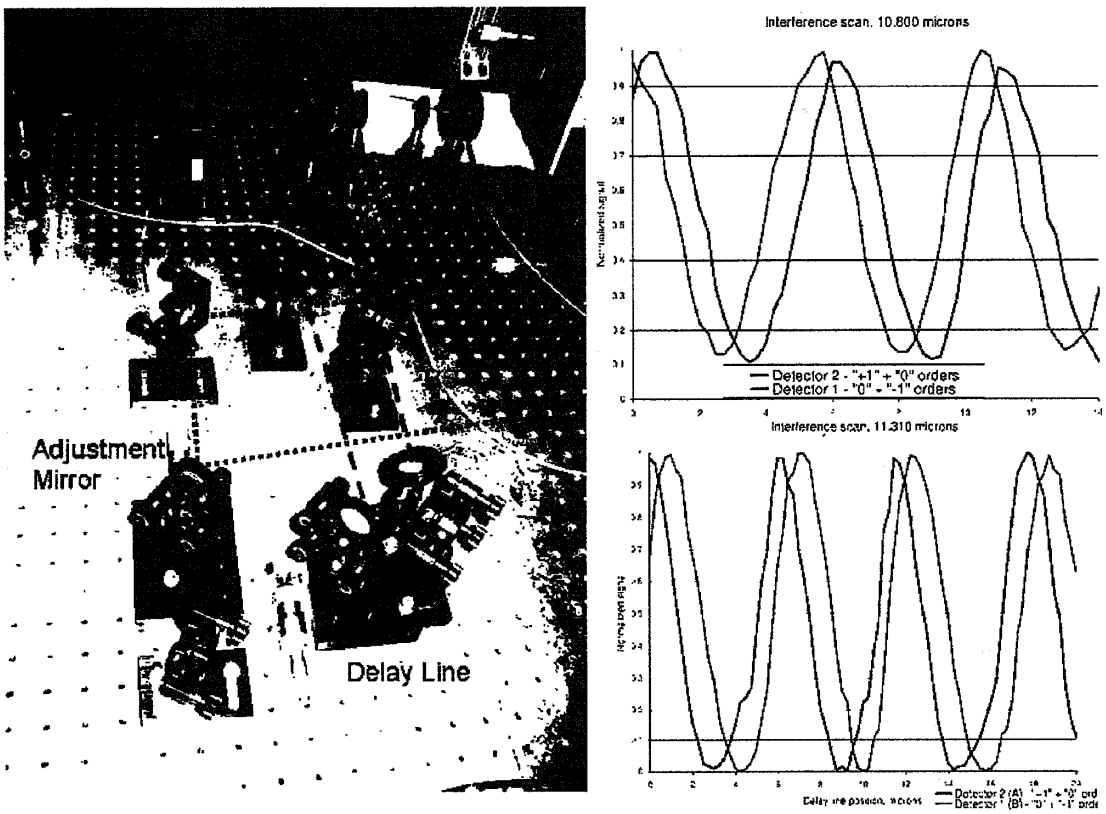


**Figure 13. (Left): Experimental Setup for 2-Beams/2-Detectors Interferometric Measurement in Our Lab. (Right): Preliminary Experimental Results**: infrared intensity on two detectors (red and black lines) are (i) different from each other; (ii) have a sinusoidal dependence on the delay line position (in microns), which is equivalent to the phase delay between the two beams; (iii) are shifted in phase by the amount equal to twice the phase difference between the 1st order (sub-diffraction) and 0th order (radiation zone) Fourier components of the bottom grating. Measurements taken at $\lambda$= 10.8 μm and $\lambda$= 11.3 μm.

With these two milestones established, it is now possible to conduct true sub-wavelength imaging experiments using two (or more) far-field detectors and jointly processing their inputs.

## Applications to Circuits and Waveguide Miniaturization: Slowing Down and Manipulating Electromagnetic Pulses (EMP) Using Advanced Metamaterials

Given the space constraints of an advanced aerospace platform and the amount of the useful payload that has to be carried, it is very important that every optical and microwave component be as small as possible. Because of the very large speed of light, there is a natural limit to how small such components can be made. Any structure capable of processing EMPs (be those optical, THz, or microwave) of temporal duration $\tau$ must be at least $L = c\tau$ long. For example, a 1 ns microwave pulse can be manipulated inside a device that is at least 1 ft long. Pulse manipulation can be understood very broadly by pulse compression, frequency shifting, harmonics generation, or other. For aerospace communications systems, it may be very desirable to have the ability to manipulate the format of EMPs, (that is, to change their frequency, duration, and repetition rate). Slowing down or even stopping the EMP can circumvent the length requirement if the group velocity is reduced to $v_g << c$, and thus the required length is $L = v_g \tau$.

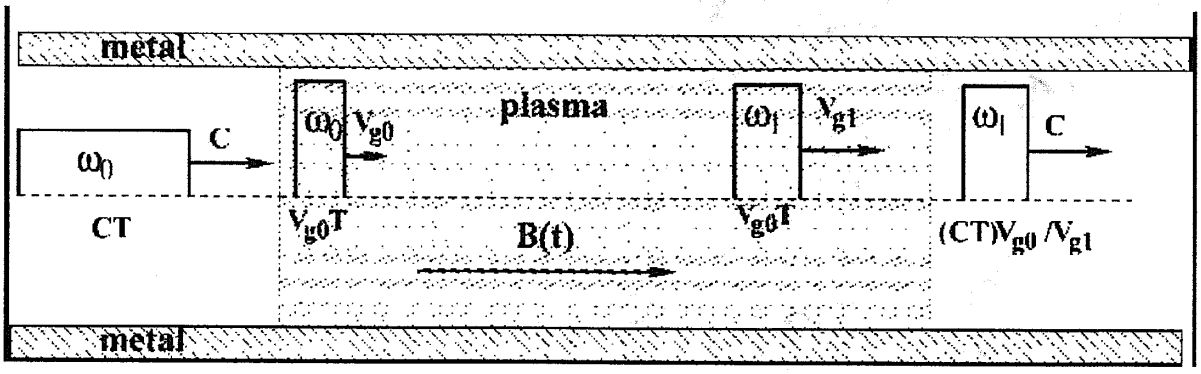


**Figure 14. Schematic of Pulse Compression in Magnetized Plasma.** A radiation pulse with initial frequency $\omega_0$ and duration $T$ slows down in the plasma to a group velocity $v_{g0} << c$. Adiabatic spatially uniform variation of the magnetic field changes the radiation frequency to $\omega_1$ and increases the group velocity to $v_{g1} >> v_{g0}$. The emerging pulse is compressed to $T_1 = T v_{g0}/v_{g1}$. (Reference 29)

An example of the pulse slowing down and subsequent manipulation is first discussed in Reference 29 in the somewhat esoteric context of magnetized plasma. Pulse duration, frequency, and (for multiple pulses) repetition rate can be controlled by storing (or slowing down) electromagnetic waves and subsequently changing the system's parameters. The essence of the compact pulse manipulator is shown in Figure 14. The pulse is slowed down inside the compact plasma device and manipulated by changing the magnitude of the magnetic field. The advantage of slowing the pulses down is three-fold. First, the device can be made smaller, resulting in size savings. Second, the temporal scale on which the system has to be manipulated is lengthened because the pulse is moving slowly. Finally, the potentially large ratio between $v_{g1} >> v_{g0}$ results in the more dramatic dynamic range of possible pulse compression ratios. Plasma-based

devices may not be appropriate in the aerospace context because of their large size, power requirements, large magnetic coils, and so forth.

Fortunately, metamaterials offer some exciting opportunities for slowing down electromagnetic waves as has been recently recognized (Reference 30). Specifically, the authors have theoretically demonstrated that an axially varying heterostructure with a metamaterial core of negative refractive index can be used to efficiently and coherently bring light to a complete standstill. One of the most remarkable aspects of the approach is that it works for relatively broadband pulses. The broadband capability is achieved through "tapering" (or axial variation) of a metamaterial's parameters such as the effective $\varepsilon$ and $\mu$. Due to tapering, each frequency component of the wave packet is stopped at a different guide thickness, leading to the spatial separation of its spectrum and the formation of a 'trapped rainbow'. In Reference 30, the authors have actually opted for a physical tapering of the waveguide (that is, reducing the thickness of the NIM waveguide along the length of the waveguide), although other approaches such as varying $\varepsilon$ and $\mu$ will also work.

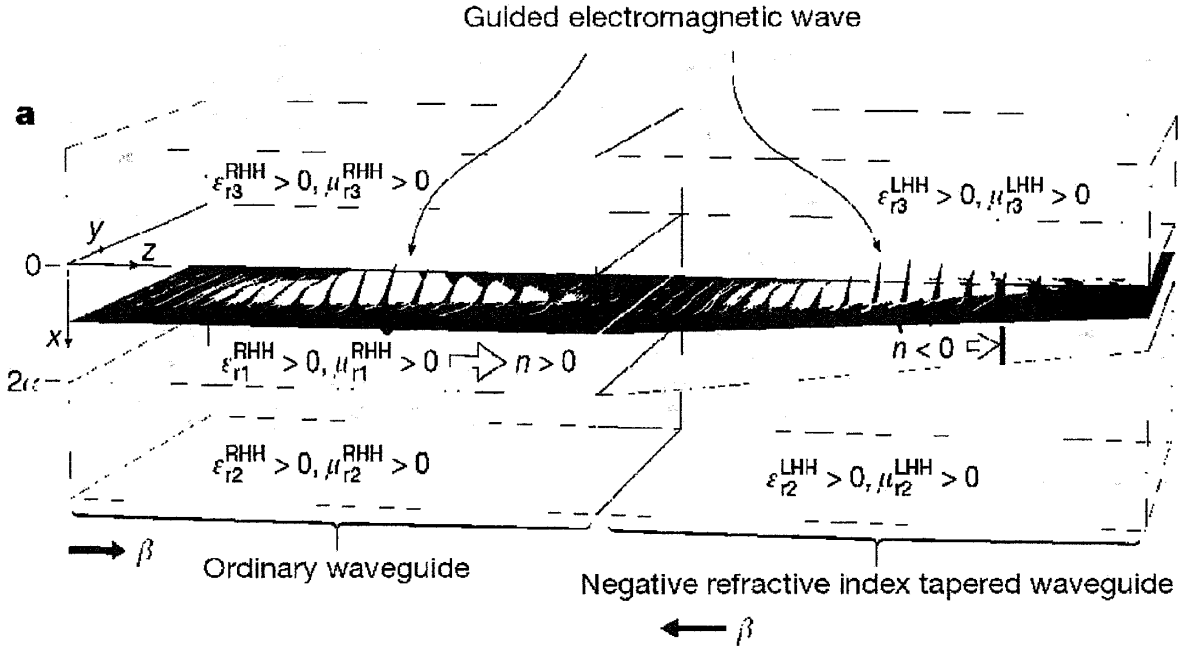


**Figure 15. Trapped Rainbow: A Waveguide with Negative Index Core Can Stop Light.** A guided wave packet is efficiently injected from the ordinary waveguide to the left-handed heterostructure LHH (see also Figure 4), inside which it propagates smoothly owing to the slow (adiabatic) reduction in the thickness of the core. The smallest (red) frequency components of the wave are stopped at the smallest core thicknesses of the LHH, while the largest (blue) components stop at correspondingly larger core thicknesses. (Reference 30)

The schematic of the light-stopping structure based on the waveguide with a negative index core (dubbed left-handed heterostructure, or LHH, in Reference 30 is shown in Figure 14. Although light stopping is possible in other guided configurations that do not necessarily require $\mu$ to be negative (for example, a metal-dielectric-metal waveguide would suffice), the key here is that perfect impedance matching can be achieved for the metamaterials-based waveguides with the negative index core. That is very important for maximizing the coupling efficiency from the regular waveguide to the LHH. Although Reference 30 does not present any specific ideas as to what could be done with the

slowed down and/or stopped light, the schematic shown in Figure 13 provides some key ideas. Moreover, the prospect of producing a low-loss negative index material in the optical domain still remains somewhat distant. Therefore, it may be worthwhile to examine other approaches to slowing down light that have emerged in the past few years.

Stopping and/or slowing down light is an old idea originating from the atomic concept of Electromagnetically Induced Transparency (EIT). The phenomenon has been considered to be purely quantum mechanical until several groups have demonstrated that it has some classical analogies (Reference 31). Remarkably, at least one group has demonstrated in the past year that EIT can be achieved using plasmonic metamaterials (Reference 32). The idea is to create a plasmonic "molecule" consisting of a radiative element coupled with a subradiant (dark) element. The plasmonic molecule showed electromagnetic response that closely resembles the electromagnetically induced transparency in an atomic system. Because of its subwavelength dimension, this electromagnetically induced transparency-like molecule was shown to be suitable as a building block to construct a "slow light" plasmonic metamaterial. The specific design of the plasmonic molecule is shown in Figure 15.

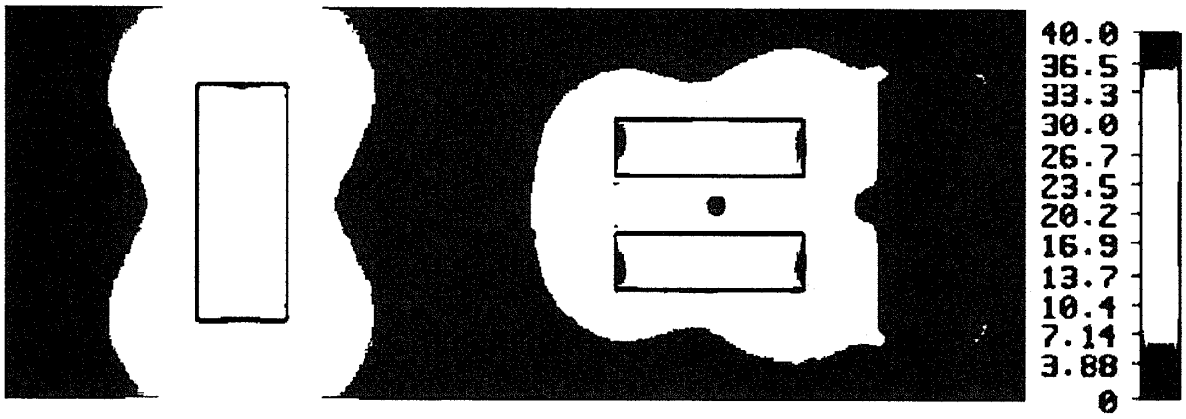


**Figure 16. "Plasmonic Molecule" Exhibiting EIT.** Left: Radiative element (metal strip) by itself gets strongly polarized by the incident EM wave, resulting in weak transmission/strong reflection. Right: Radiative element coupled to the "dark" element (two strips). Dark element possesses a non-radiative quadrupole resonance which is excited by the radiative element and de-polarizes the radiative element. The result: vanishing reflection, high transmission. Color bar: $|\vec{E}|$ normalized to the incident laser field at $\lambda$ = 700 nm. (Reference 32)

This specific plasmonic molecule consists of the "dark state" (two parallel plasmonic antennas oriented perpendicular to the incident vertical electric field) and the "radiative state" (single plasmonic antenna oriented parallel to the electric field). The quality factor of the "dark antenna" state is an order of magnitude higher than that of the "radiative" antenna. When the "radiative" antenna is spatially separated from the "dark" antenna (or when the dark antennas are not present at all), all or most of the incident radiation is reflected from an array of "radiative" antennas whenever the resonance frequency of the antenna coincides with that of the laser. In this example, the long antenna is 128 nm long, and the resonance wavelength is at $\lambda$ = 700 nm. The key effect here is that the resonance of the "dark" antenna should be at the same wavelength.

Because the exploited resonance has a quadrupole nature, it is slightly red-shifted. For that reason, the length of the "dark" antenna is 100 nm. When the two antennas are brought together, the radiative antenna polarizes the dark antenna, which, in turn, depolarizes the radiative antenna. As a result, the dipole moment of the coupled system is drastically reduced, the reflection drops and transmission increases to almost 100 percent (limited only by losses). Most of the energy is now stored inside the non-radiative (dark) antenna.

If multiple layers of dark/bright antennas are employed as shown in Figure 16, then one can achieve one of the most important manifestations of EIT; "slow" light. Slow light can have many interesting technological applications because (a) slow light is easy to manipulate by changing the structure's parameters (as described in the section on tunable metamaterials), and (b) slow light has a high field intensity (enhanced by the ratio of the free-space propagation speed to the slow propagation speed), therefore, all nonlinear processes are enhanced for slow light. Such nonlinear processes may include harmonics generation, optical diode action (see the section on non-reciprocal optical elements), and many others.

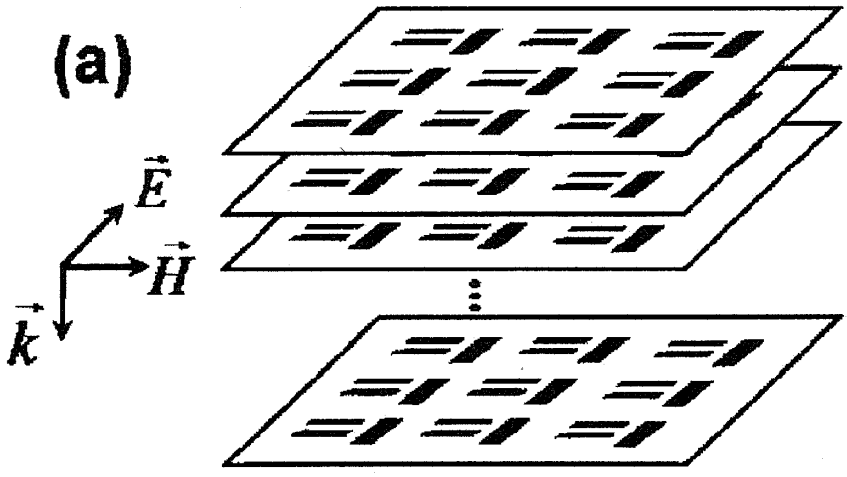


**Figure 17. True Multi-Layer Metamaterial With a Unit Cell Shown in Figure 15:** radiative antenna (single metal strip) coupled to a dark antenna (two perpendicular metal bars). Such metamaterial exhibits "slow" light propagation along the incidence direction (slowed down by a factor 30 or more). (Reference 32)

It is important to realize that the geometry suggested in Reference 32 is not unique. For example, the dark and radiative antennas need not reside in the same plane. Nor is the effect of EIT (and the related phenomenon of slow light) limited to the optical domain. Both infrared and microwave-range designs have started emerging. These frequency domains are likely to be of greater use for advanced aerospace platforms than the visible range targeted by most studies.

## Metamaterials for Energy Harvesting

One of the most important applications of metamaterials is related to developing "perfect absorbers" of infrared electromagnetic radiation, be it in the mid-to-long infrared part of the spectrum (making it relevant for night vision, harvesting of the Earth glow mid-infrared radiation, and so forth) or in the near-to-mid-IR spectrum (making it relevant for day-time infrared photography of the earth terrain). For example, day-time infrared photography relies on the different sunlight reflectivities of surfaces (for example, snow, brick walls, concrete walls, grass, and so forth), and can easily distinguish between those surfaces. This reflectivity differential tends to be the greatest between 2-3 microns, and rapidly decays toward longer wavelengths. Open sky contains very little infrared radiation which explains why infrared imaging/photography is very important for aerial and satellite surveys. Because light scattering in the atmosphere scales as $\lambda^{-4}$, imaging through the atmosphere in the visible range is impossible, and infrared imaging becomes important. This is especially true for the $1 < \lambda < 4$ μm range. For longer wavelengths ($\lambda > 10$ μm) this brightness differential is largely gone because the emission spectrum is dominated by thermal emission. In fact, the Earth glow maximum is around $\lambda > 10$ μm, with most of the energy contained in the 3 μm $< \lambda <$ 14 μm range. This longer wavelength (mid-to-far IR) spectral range is also very important. It can be used for night-time energy scavenging by high-altitude satellites and other aerospace platforms.

There has been a surge of activity in this area, first in the microwave/THz part of the electromagnetic spectrum (References 33, 34), and subsequently in mid-to-far infrared (Reference 20). The concept of narrow-band metamaterials-based absorbers introduced in Reference 33 has the potential for developing highly efficient bolometer arrays. When applied to the infrared part of the spectrum, it can be used for space navigation, especially when weak infrared signals from specific stellar objects need to be picked up and discriminated from other radiation sources. For such applications, the narrow-band "perfect" absorption is highly suitable. An array of such bolometers would reject (reflect) all undesirable frequencies and focus on the single wavelength characteristic of the source of interest. Moreover, if an array of different (for example, tuned to different frequencies) narrow band detectors can be deployed, then the hyper-spectral imaging capability could bring additional benefits. For example, absolute temperatures of a radiation source (that is, stellar bodies) could be accurately determined, and could improve the accuracy of space navigation further.

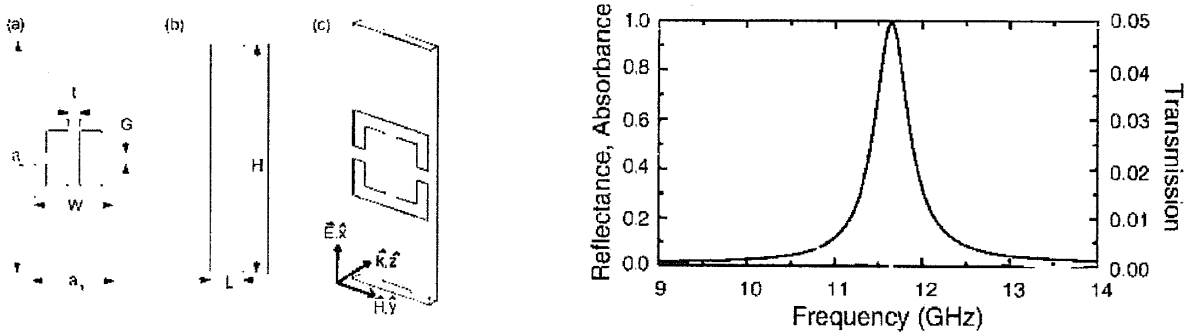


**Figure 18. "Perfect" Narrow-Band Microwave Absorber.** (a-c): Unit cell design. Right panel: simulated absorption/transmission/reflection. (Reference 33)

One possible design for the microwave frequency band is shown in Figure 17. High absorption is accomplished by reducing reflections to zero. This is accomplished by choosing metamaterials parameters such that $\varepsilon_{eff}(\omega_r) = \mu_{eff}(\omega_r)$ at the resonant frequency $\omega_r$. Note that both the real and imaginary parts of the permittivity and permeability must be equal to each other, and that the imaginary parts don't necessarily need to be small for absorber applications. In fact, it is desirable that they are not too small, thereby enabling 100 percent absorption within a single layer of metamaterial. The above design can be scaled down to the THz range, as was later demonstrated in Reference 34. It is difficult to find strongly absorbing materials at THz frequencies that are compatible with standard photolithography. Thus, a potential application of these metamaterial structures is as absorbing elements in thermal detectors. A strong absorption coefficient is also necessary to have a small thermal mass. This is important for optimizing the temporal response of thermal detectors. The metamaterial presented here has a 6 micron thick film (that is, λ/50 thickness for THz radiation) and 70 percent absorptivity, which yields an absorption coefficient of 2000 $cm^{-1}$.

One drawback of the original design was the narrow angular range of the absorber. The absorption dropped dramatically when the incidence angle was as small as 20 degrees. The reason for that is a relatively large unit cell of the metamaterial. In fact, when the unit cell size is larger or comparable to λ/2n, where n is the refractive index of the substrate, it is inappropriate to call such structure a "metamaterial". A true impedance-matched metamaterial would, in fact, always have a very broad angular response.

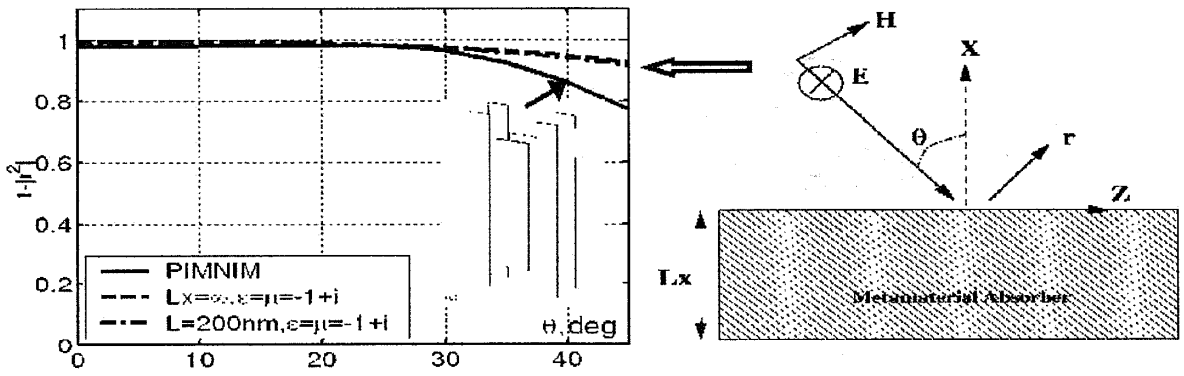


**Figure 19. Wide-Angle Plasmonic Absorber Based on Negative Index Metamaterial.** Right panel: schematic of an absorption-measuring experiment. A generic metamaterial with $\varepsilon_{yy} = \mu_{zz} = -1 + i$, $\mu_{xx} = 1$ is assumed. Left panel: angular dependence of the absorption for a generic and specific (shown in the inset) metamaterial. Both exhibit wide-angle absorptivity. (Reference 20)

This fact can be expressed by a simple formula for the absorption coefficient $A$ (Reference 20):

$$A = 1 - \left| \frac{\cos\theta - \sqrt{\varepsilon_{yy}/\mu_{zz} - \sin^2\theta/(\mu_{xx}\mu_{zz})}}{\cos\theta + \sqrt{\varepsilon_{yy}/\mu_{zz} - \sin^2\theta/(\mu_{xx}\mu_{zz})}} \right|^2 \quad (4)$$

where we've assumed that, for normal incidence, this metamaterial is impedance-matched: $\varepsilon_{yy} = \mu_{zz} = -1 + i$. Equation 4 can be simplified under the assumption of $|\varepsilon_{yy}| >> 1, \mu_{xx} = 1 : A \approx 1 - \tan^4(\theta/2)$, implying that $A \approx 0.97$ even for $\theta = \pi/6$. The challenge, if course, is to design a true impedance-matched optical metamaterial. Success has been achieved in designing such a metamaterial (Reference 20).

The recently published design is shown in Figure 19. The unit cell consists of two layers of plasmonic antennas; the cut-wire antenna that imparts magnetic (as well as some electric) response to this metamaterial, and the continuous-wire antennas that impart a purely electric response. It is found that the wide-angle capability could be very important for several applications. Wide-angle power absorption efficiency is desirable for miniaturizing photodetectors or microbolometers down to the wavelength size.

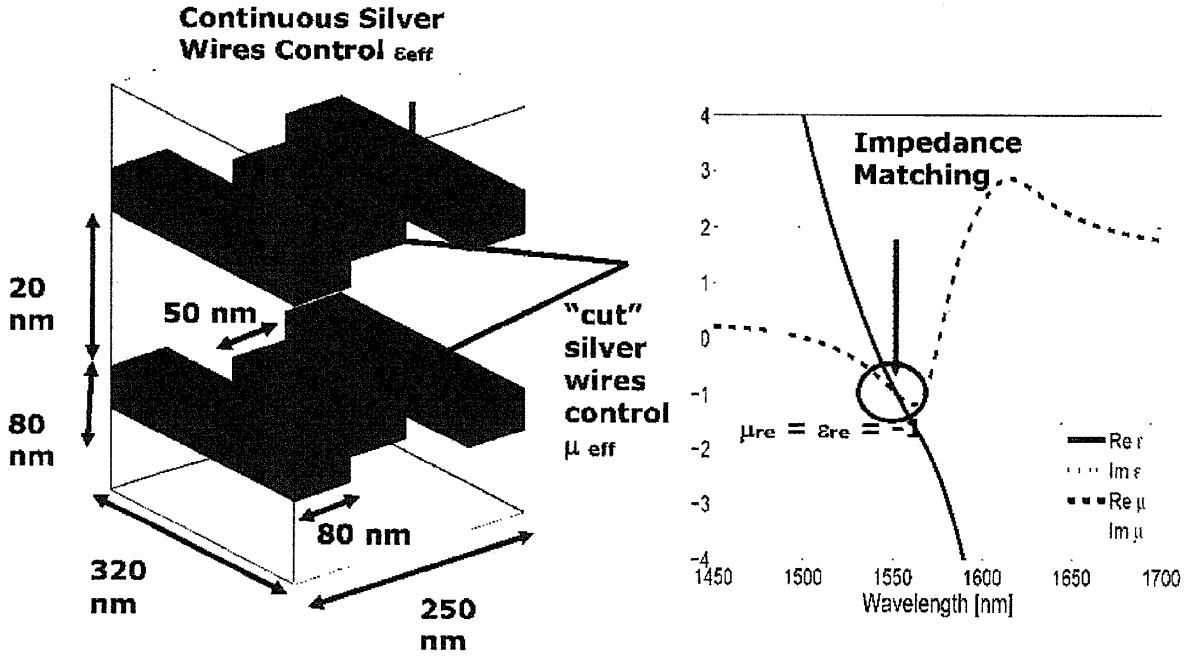


**Figure 20. Specific Design of a Wide-Angle Plasmonic Absorber Based on Negative Index Metamaterial Operating at λ=1550 nm.** Left panel: Schematic of the silver-based plamonic structure. Right panel: Extracted permittivity and permeability for the normal incidence demonstrate impedance matching: $\varepsilon_{yy} = \mu_{zz} = -1 + i$. (Reference 20)

For example, to focus light on a wavelength-sized photodetector or micro-bolometer requires high-NA optics (a NA=0.5 or higher). Therefore, a photodetector should be able to absorb light incident at 30 degree angle. For advanced aerospace platforms it is easy to envision a scenario where an airborne platform is powered by a high-power infrared laser source located on Earth. If the wavelength falls inside the transparency window of the atmosphere (between 3 and 4 μm, and also around 10 μm), then such a

prospect is not too farfetched because scattering in mid-infrared by atmospheric gases is essentially zero. For such a remote powering scenario to be feasible, one would need a highly efficient absorber at the specific wavelength corresponding to that of the source. Moreover, as the space platform is moving, it is desirable that the absorption remain high even for non-normal incidence angles.

The second application is for thermophotovoltaics (TPV) (Reference 35). Some type of thermophotovoltaic converter will almost undoubtedly be installed on the advanced aerospace platforms of the future. Presently even advanced (experimental) electric cars are using TPV cells to convert the heat from their engines into electricity. Such converters have already been shown to be capable of increasing the range of electric vehicles by a factor of 3. We believe that metamaterials could play an important role in developing highly efficient TPV cells. By virtue of Kirchhoff's law, emissivity of a thermal emitter approaches the blackbody limit only if the absorptivity approaches unity. Moreover, wavelength-selective radiators can dramatically improve the efficiency of current generation in a TPV cell if their emission spectrum is matched to the bandgap of the TPV converter. For example, a typical TPV converter, GaSb, has the bandgap of EG = 0.7 eV that would be ideally suited to a wavelength-selective radiator operating in near infrared around $\lambda$ = 1.7 μm.

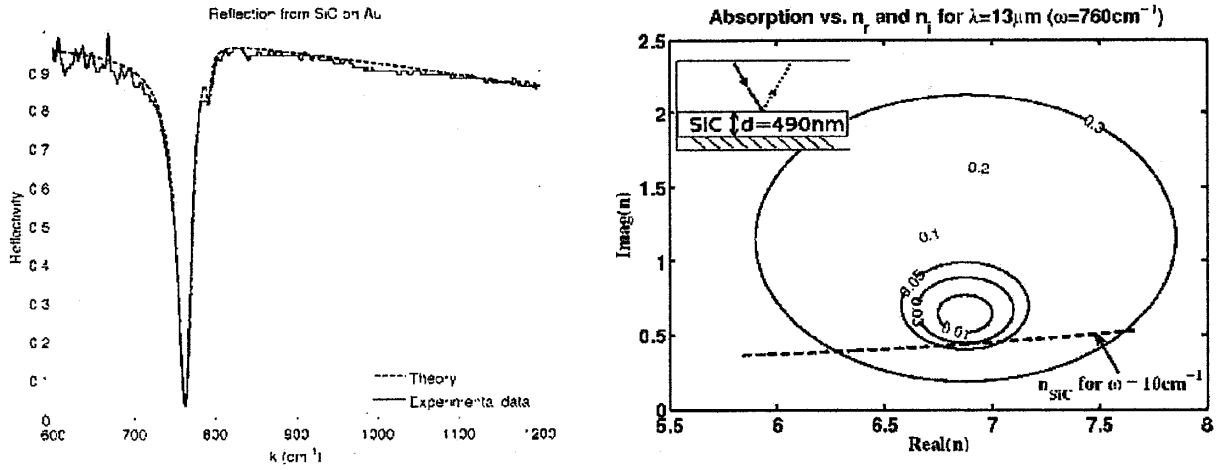


**Figure 21. (Left) Experimental Result, Reflectivity Versus Wavelength, that Inspired the Proposed Effort: A Modestly Absorbing Material (SiC) Turns Into a "Perfect Mid-IR Absorber" When a λ/4 -Thick SiC Film Is Backed by a Metal Mirror. (Right): Theoretical Plot – Constant Reflectivity Contours Plotted in the (Real(n), Imag(n)) Space.** High material absorptivity Imag(n) is required to achieve perfect absorption (R=0). Posed question: can a metamaterials-based semi-transparent mirror enhance absorption and result in an almost-perfect ultra-thin absorber?

The perfect absorbers shown in Figures 17-19 may be too complex for practical applications. Metamaterials tend to be lossy because of the large field concentration in the metal. Therefore, work has recently started working on a new type of metamaterial (so-called CMMs mentioned in the Introduction), that could potentially make weakly-absorbing semiconductors (that is, Si in the visible) absorb much stronger. The goal here is to make a thin (although not necessarily a very sub-wavelength) absorber backed up by a sheet of CMMs which would prevent reflections and result in a very high absorption. Applications that are considered are essentially the same as for the "perfect" absorbers described above. For example, satellites can use the Earth glow for nighttime battery recharging. The collected power is quite high; 1 $m^2$ of black surface at

room temperature radiates 460 W. Earth-based powerful mid-infrared sources can be used for nighttime powering of airborne platforms.

All these applications would benefit from the following components: (a) perfect absorbers of infrared radiation that can be installed on the receiving platforms, (b) efficient sources of thermal mid-infrared radiation. These two components are related to each other. Therefore, developing an ultra-thin perfect absorber of infrared radiation would be highly desirable. The ultra-thin aspect is important because it enhances the radiation-to-electricity conversion efficiency. For example, it is well known that carrier separation-collection efficiency in a solar cell improves as the cell gets thinner. The challenge is to combine this carrier separation-collection efficiency with sufficient absorption. Unfortunately, the absorption length of many semiconductors in the infrared is fairly small. Recent experiments provide the new metamaterials-based concept for increasing the absorptivity of otherwise semi-transparent materials. Below some of the (still unpublished) experiments and theoretical developments that might result in new metamaterials-based perfect absorbers are described.

Figure 20 (left) indicates a very instructive experimental result: reflectivity $R$ from an ultra-thin (500 nm) SiC film backed up by a metal mirror. At $\omega = 762\ \mathrm{cm}^{-1}$ (or $\lambda = 13.1$ μm) reflectivity from the structure is less than 3 percent. That implies 97 percent absorption in a film of thickness $d = \lambda/25$ . This remarkable absorptivity can be explained using the well-known microwave concept: the Salisbury screen. It turns out that at $\lambda = 13.1$ μm film thickness is $d = \lambda/4n$, where $n = n_{re} + in_{im}$ is the complex refractive index of SiC. A simple formula for the reflectivity from a metal-backed thin film can be derived:

$$R = \left| \frac{r_0 - e^{2i\delta}}{1 - r_0 e^{2i\delta}} \right|^2 \tag{5}$$

where $r_0 = \dfrac{n-1}{n+1}$ is the reflection coefficient from the air/SiC interface and $\delta = nk_0 d$ is the complex phase shift across the film which includes losses. Fixing the laser frequency $\omega = ck_0$ and the sample's thickness $d$ , we can plot the reflectivity as a function of $re(n)$ and $im(n)$. As can be clearly seen from Figure 20 (right), there is a "sweet spot" corresponding to specific values of $re(n)$ and $im(n)$ that results in vanishing reflectivity (or perfect absorption). $R$ vanishes when the quarter-wavelength condition is approximately satisfied:

$$re(n)k_0 d = (2m+1)/2 \tag{6}$$

where $m$ is an integer. Finite reflection and imperfect absorption result from lower (or higher) values of $im(n)$. Note that, coincidentally, for the case of heavily doped SiC predicted reflection is only 3 percent. However, for most materials (that is, Si for visible light) absorption is too low for perfect absorption. Therefore, a question is posed: Can one modify the structure of the metal screen to enhance absorption? It is CMMs that enable such functionality?

Specifically, it has been found that by making the mirror slightly leaky, we can actually increase absorption. If the reflection coefficient of a mirror is given by $r_2$, then the reflection/transmission coefficients $r,t$ through the structure are given by:

$$r = \frac{r_0 + r_2 e^{2i\delta}}{1 + r_0 r_2 e^{2i\delta}}, t = \frac{t_0 t_2 e^{i\delta}}{1 + r_0 r_2 e^{2i\delta}} \quad (7)$$

where $t_2 = 1 + r_2$ and $t_0 = 1 + r_0$. Note that Equation 7 turns into Equation 6 if $r_2 = -1$ (perfectly reflecting mirror). From Equation 7 it follows that it may be possible to engineer the reflectivity $r_2$ in such a way that minimizes reflection $|r|^2$ while keeping transmission $|t|^2$ small. The remainder of the energy is guaranteed to be absorbed by the quarter-wavelength thick absorber.

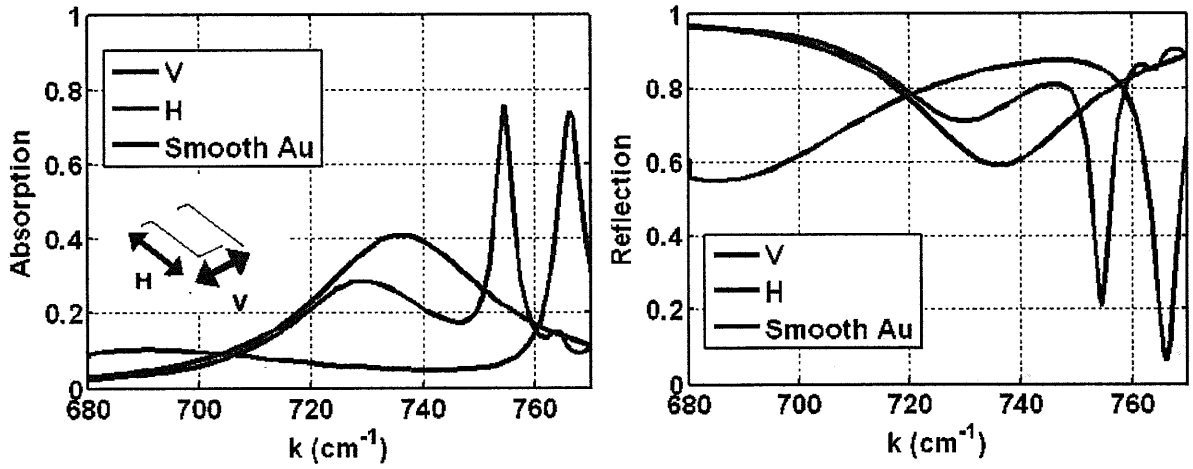


**Figure 22. Preliminary Attempts to Design a Better Absorber Using Complementary MetaMaterials (U-shaped CMM).** Note that only 40 percent absorptivity is possible with a smooth gold film. Paradoxically, this absorptivity increases to 75 percent when the metal mirror is made "leaky" by perforating it with an array of CMMs (left panel).

The design process for engineering $r_2$ using the simplest CMMs, U-shaped apertures, has been started. Some of the preliminary results are shown in Figure 22. Figure 22 illustrates how the (relatively low) 40 percent absorptivity of the SiC film covered by a smooth Au mirror (black line) can be boosted up to 75 percent by patterning the mirror using CMMs. We call such a "leaky mirror" patterned by CMMs a *MetaMirror*. It is clear from Figure 23 that a MetaMirror can be used for making absorptivity polarization-dependent (if that is desirable for applications demanding a reflector-polarizer). MetaMirror can also be used for shifting the absorption wavelength which would be highly desirable for developing broadband absorbers. We have found that there are two mechanisms capable of making MetaMirrors: (a) excitation of the Long Range Surface Plasmon Polaritons (LR-SPPs) on the patterned MetaMirror, and (b) excitation of highly-localized (shape-dependent but period-independent) SPPs. An example of the mechanism (a) is shown in Figure 23, but we also have preliminary results indicating that both mechanisms can be operational in the same MetaMirror for close-by frequencies resulting in multiple dips of the reflectivity coefficient $|r_2|$. By comparing

Figure 23 with Figure 22, it is observed that the dips correlate with drops of the total reflectivity and increases of the total absorption of the absorber/MetaMirror structure.

The MetaMirror approach to infrared energy harvesting is one of the very promising applications of metamaterials. A number of aspects of MetaMirrors must be investigated and several important questions must be answered before practical applications can be pursued. Some of those questions are:

- What is the angular dependence of absorptivity, and can it be made wide-angle as we have recently demonstrated in Reference 20 for negative-index metamaterials?
- Can absorptivity be made broad-bandwidth by combining localized resonances with the LR-SPPs? That could be potentially accomplished by using U-shapes with different geometries, yet spaced in a regular periodic pattern, or by using quasi-periodic arrangements of CMMs shapes.
- What are the most promising polarization-independent unit cells of CMMs that result in enhanced absorptivity?
- Is it possible to apply the MetaMirror concept in the visible and contribute to solar energy harvesting?

As more researchers are investigating energy-harvesting applications of CMMs (or MetaMirrors), it is believed that these questions will be answered very soon.

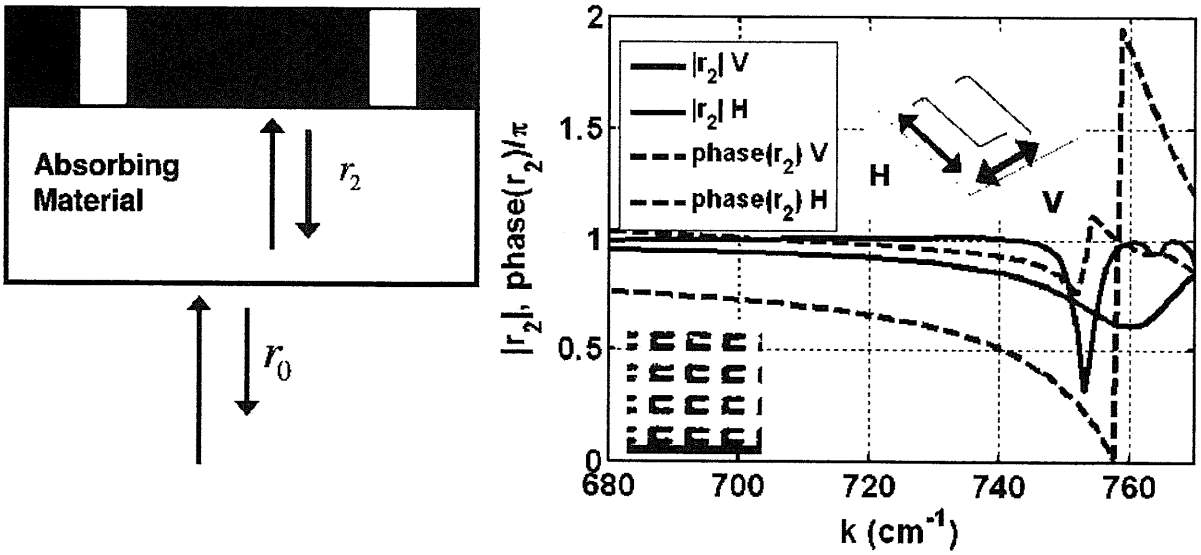


**Figure 23. Engineering the Complex Reflectivity Coefficient $r_2$ Defined on the Left Panel Using the Concept of a MetaMirror.** Dips of $|r_2|$ shown in the right panel correspond to reflection dips (and absorption peaks) in Figure 2. The physical reason for these dips is the excitation of long-range SPPs on the MetaMirror surface. Inset: Fabricated MetaMirror.

## Nonlinear Non-Reciprocal Chiral Metamaterials: For Developing Novel Optical Isolators and "One-Way" Microwave Mirrors

Optical isolators play a pivotal role in fiber-optic communication systems by protecting their active components ( for example, optical amplifiers) from unwanted reflected signals that could potentially destabilize them. Such protection is especially important in the context of advanced aerospace platforms, where repairs must be avoided at all costs. At the core of isolator design is an element which provides non-reciprocity by breaking time reversal symmetry. Non-reciprocity can only be caused by magnetic fields or nonlinearities. The most common approach using magnetic Faraday rotators results in a rather bulky implementation of an isolator. It is believed that metamaterials are uniquely positioned to enhance the other approach of breaking non-reciprocity: use of nonlinear effects. It is very natural to use metamaterial in the context of enhancing nonlinearity. As was explained previously, metamaterials can be used to slow down light and, therefore, compress electromagnetic energy. Any intensity enhancement increases nonlinear effects, and larger nonlinear effects translate into more compact devices. Another aspect that makes metamaterials very appealing for non-reciprocal applications is the ability to make their properties tunable to almost any frequency range.

One concept that is being explored (still unpublished) relies on the nonlinearity and several other aspects of engineered chiral metamaterials. A novel type of a nonlinear optical isolator based on adiabatic time-irreversible mode conversion (ATIMC) between two electromagnetic modes supported by the chiral metamaterial is envisioned. As an example of such metamaterial, a twisted optical fiber shown in Figure 24 is used. It supports a tightly-confined core mode (CoM) which can be coupled to/converted into a loosely confined cladding mode (ClM) of the same fiber. Coupling and conversion between the core and cladding modes is accomplished by twisting the fiber with a variable pitch $\Lambda(z)=2\pi/\beta_{\alpha}$. Time irreversibility is achieved due to the combination of the Kerr nonlinearity of the core material (resulting in the intensity-dependent propagation constant of the CoM) and small but finite loss of the ClM. As a result, the CoM, when injected in the *forward* direction, passes through the isolator with a negligible conversion into the ClM. If subsequently reflected back into the isolator (this is equivalent to time reversal), it gets entirely converted into the ClM and subsequently damped as illustrated by Figure 25. Preliminary simulations indicate that, for sufficiently large nonlinearity, one can find the loss rate $\alpha$ for the ClM such that two conditions are satisfied: (a) $\alpha$ is small enough so that virtually no power is lost in the forward direction, and (b) $\alpha$ is large enough so that the time-reversal is strongly violated, resulting in near-perfect optical isolation.

**Figure 24. Example of a Generic Chiral Metamaterial:** An Optical Fiber with a Rectangular Cross Section Core Twisted During the Drawing Process Forms a Double Helix. If the core index is nonlinear, then one can engineer a variable helix pitch in such a way that the core (localized) modes can be selectively coupled to cladding modes depending on the direction of propagation.

Under a highly simplified assumption of just two interacting mode (core and cladding), we have developed a coupled-mode theory describing the evolution of the mode amplitudes $a_{co}$ and $a_{cl}$ along the fiber axis $z$. The set of the generic equations for $a_{co}$ and $a_{cl}$ is given by:

$$\begin{aligned} &\frac{\partial a_{co}}{\partial \tau} - i(\beta_0 + \gamma |a_{co}|^2 - \delta/2)a_{co} = iWa_{cl}, \\ &\frac{\partial a_{cl}}{\partial \tau} - i(\beta_0 + \delta/2)a_{cl} = iW^* a_{co} \end{aligned} \qquad (8)$$

where $\beta_0 = c(\beta_{c0} + \beta_{cl})/2\omega$ is the average normalized propagation constant, $\delta(\tau) = c(\beta_{c0} - \beta_{cl} + 2\beta_u)/\omega$ is the distance-dependent mode detuning, $\gamma$ is the nonlinearity coefficient, $W$ is the coupling strength between the modes, and $\tau = \omega z/c$ is the normalized propagation distance.

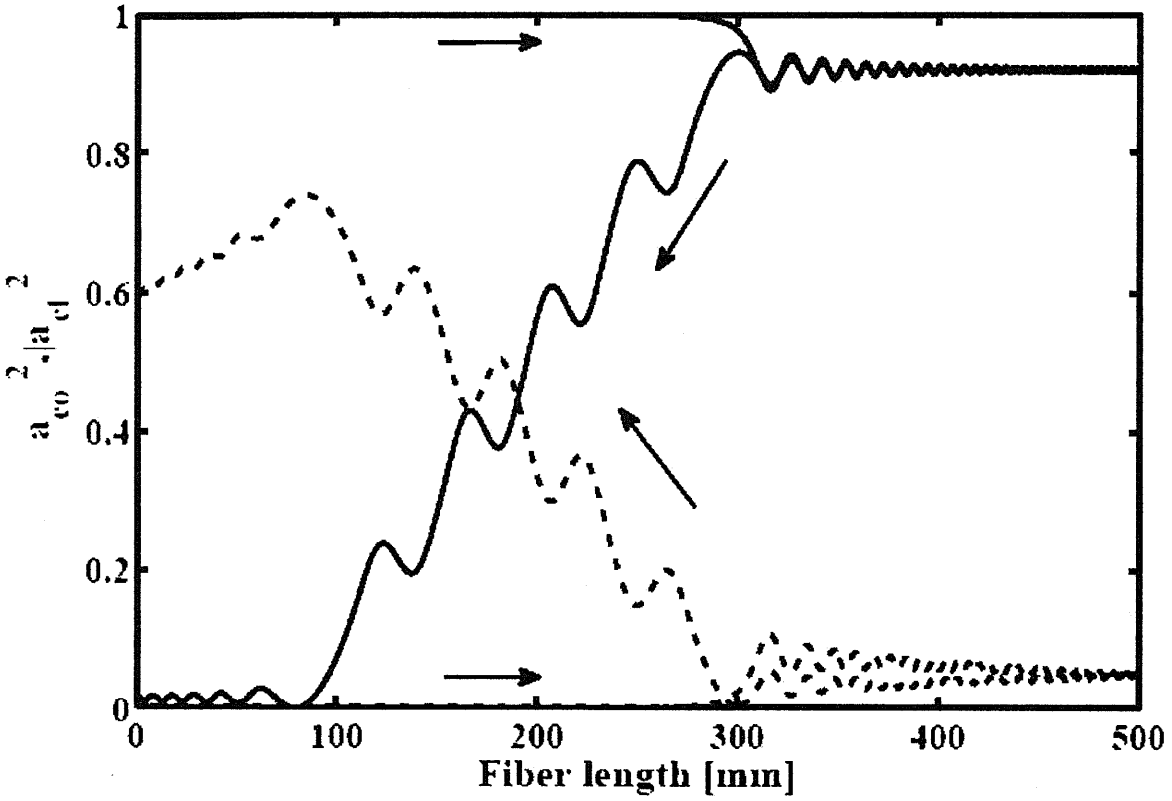


**Figure 25. Example of Time-Irreversibility of Light Propagation Inside the Twisted Fiber Core:** the core mode propagates with almost no loss from left to right (purple solid line), reflects back, and gets dissipated/mode converted on its way back (red line). Input mode is assumed to be right-hand circularly polarized (RCP). Mode conversion: into LCP cladding mode (dashed line). Propagation from left to right is represented by the red lines, from right to left: by the purple lines.

As an example, we have used a Chiral Fiber (CF) with the following properties: a 2 μm x 1.8 μm elliptical core with refractive index of $n_{co} = 2.2$ surrounded by a round cladding with radius $R = 20$ μm and refractive index $n_{cl} = 2.15$. The helical pitch is assumed to linearly vary over $l_{max} = 500$ mm by 6 percent around $\Lambda = 166$ μm. The assumed $\gamma$ corresponds to the nonlinear refractive index $n_2 = 5.4 \times 10^{-16}$ m$^2$/W at the operating vacuum wavelength $\lambda$ = 1.5 μm and the peak power P = 3.5 W. The cladding mode was assumed to be lossy with the loss coefficient $\alpha$ = 10 dB/m . Results are shown in Figure 25. A core mode injected from the left end of the fiber (z = 0) propagates through the fiber without converting into the cladding mode (purple solid line) with minimal losses. After getting reflected at z = 500 mm, the principal core mode (red solid line) gets converted into the delocalized cladding mode (red dashed line) and damped out. This example clearly demonstrates that the interplay between mode-coupling, nonlinearity, and losses can result in the dramatic loss of time-reversal.

Future research will be looking at other metamaterial systems that support two distinct modes (one with a strongly nonlinear response and strong spatial localization, the other essentially linear and delocalized), orthogonal polarizations, and investigate non-reciprocal wave propagation in such metamaterials. Structures from the previous

sections, such as shown in Figures 15 and 16, will be primary candidates for implementing optical and microwave non-reciprocity. Such metamaterials would be comprised of a unit cell containing a non-radiative element (that is, a two-strip capacitor-loaded antenna supporting a "dark" magnetic mode) and a single "bright" dipole antenna. Such a system exhibits EIT when the frequencies of the "dark" and "bright" resonances coincide. EIT results in energy compression and enhanced nonlinearity. The source of the nonlinearity could be, for example, a variable capacitance diode (varactor) used as a capacitive load of the double-strip antenna. The second (linear) mode could have an orthogonal polarization, and the coupling between the two could be accomplished via spatially-periodic displacement of the single-strip and double-strip antennas with respect to each other.

## Tunable Switchable Metamaterials

Electromagnetic properties of most metamaterials are "hard-wired", meaning they are determined during fabrication. That can be a serious impediment to using them in the context of space exploration. Being able to change optical/electromagnetic properties of a metamaterials-based device without having to re-manufacture it would be highly desirable. Therefore, this survey is concluded by describing some of the recent progress in making reconfigurable/switchable metamaterials. This is a new exciting area of metamaterials research that is worth watching for applications. One of the first electrically-controllable THz metamaterials has been reported in Reference 36, where resonant properties of the electric split ring were controlled by applying reverse bias between metal and highly-doped in GaAs layer. The schematic of the experiment is shown in Figure 25. Without reverse bias there is no resonant response of the split ring to incident THz pulse because highly-conductive electrons of the n-GaAs layer are shorting the gap of the resonant split ring as schematically indicated in Figure 26(b). With the applied reverse bias, electron density is depleted inside the gap. The resulting transmission spectrum shows spectral dips which were converted into the effective dielectric permittivity $\varepsilon_{eff}(\omega)$ that exhibited resonant peaks. The strongest of the peaks corresponded to the Inductance-Capacitance (LC) resonance of the split ring. One possible application of such electrically tunable metamaterial suggested in Reference 36 was a modulator. The authors claim that the performance of their device as a *THz* modulator already exceeds current state-of-the-art electrical THz modulators (based on semiconductor structures) by one order of magnitude on resonance. Moreover, their device operates at room temperature. Needless to say, this metamaterial-based modulator can be improved. For example, configurations exploiting EIT could result in stronger modulation strength.

Another interesting possibility for tuning microwave metamaterials has been suggested in Reference 37. Ferroelectrics (such as BST) can be tuned by applying DC voltage which changes their dielectric permittivity. This property of BST was utilized to develop frequency tunable magnetic metamaterials using metallic split rings loaded with barium-strontium titanate thin film capacitors. The resonant frequency of this medium is voltage tunable across a 140 MHz band centered at 1.75 GHz. The effective relative permeability of the slab was shown to have Lorentzian shape that reaches minimum values between $-2$ and $-3$ for biases from 0 to 5 V. Therefore, permeability of the slab can tune between positive and negative values, making it useful in applications requiring a state switchable magnetic permeability.

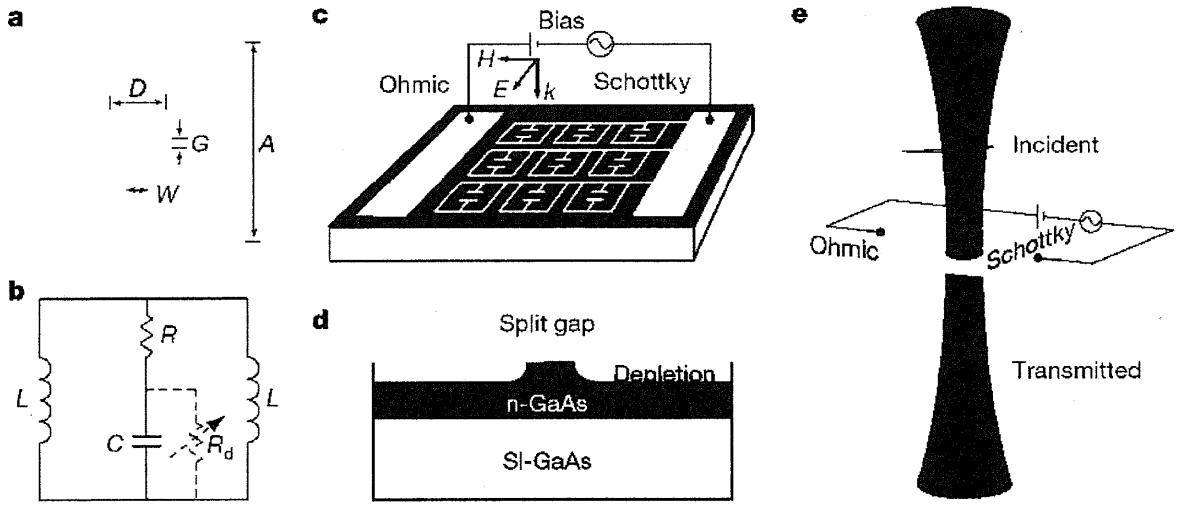


**Figure 26. *THz* Properties of an Electric Split Ring Resonator.** (a) Are controlled by applying voltage between Schottky and Ohmic contacts (c,d). (b) Schematic of circuit with inductance. Applied voltage controls charge density inside the split gap (d). The structure is investigated using a single-cycle THz pulse (e). (Reference 36)

## Summary and Conclusions

While it is difficult to pinpoint the exact applications that metamaterials will find in advanced aerospace industry, metamaterials possess several features that uniquely suit them for aerospace applications. First, they enable miniaturization of a variety of optical components. Making space-born devices small and light-weight is essential. These opportunities have been covered in detail. Second, metamaterials enable new modalities for sub-diffraction imaging: super-lenses, hyperlenses, and far-field superlenses. Those modalities dispense with the near-field scanning microscopes, which are complex, slow-scanning, large devices that are not appropriate for advanced aerospace platforms. Harvesting infrared photons, whether from coherent laser sources on Earth (for guidance, energy recharging, and so forth), from thermal Earth glow, or from the stars, is likely to be important for aerospace platforms. Metamaterials offer unique opportunities for making efficient wavelength-tunable, wide-angle absorbers. As discussed in the numerous examples in this report, metamaterials are going to revolutionize the way light is captured, manipulated, and used for imaging. Although metamaterials are still an academic area of research, these examples illustrate that there is great potential for practical applications.

## References

[1] Smith D R, Padilla W J, Vier D C, Nemat-Nasser S C, Schultz S 2000 PRL 84 4184.

[2] J. B. Pendry, "A Chiral Route to Negative Refraction", Science 306, 1353 (2004).

[3] D. Schurig and D. R. Smith, "Spatial filtering using media with indefinite permittivity and permeability tensors", Appl. Phys. Lett., 82, 2215 (2003).

[4] D. R. Smith and D. Schurig, " Electromagnetic wave propagation in media with indefinite permittivity and permeability tensors", Phys. Rev. Lett., 90, 77405 (2003)

[5] A. Alu, M. G. Silveirinha, A. Salandrino, and N. Engheta, "Epsilon-Near-Zero Metamaterials and Electromagnetic Sources: Tailoring the Radiation Phase Pattern," Physical Review B 75, 155410 (2007).

[6] D. Schurig, J. J. Mock, B. J. Justice, S. A. Cummer, J. B. Pendry, A. F. Starr, D. R. Smith, "Metamaterial Electromagnetic Cloak at Microwave Frequencies", Science 314, 977 (2006).

[7] Hu Tao, Nathan I. Landy, Christopher M. Bingham, Xin Zhang,Richard D. Averitt, and Willie J. Padilla, "A metamaterial absorber for the terahertz regime: Design, fabrication and characterization", Opt. Express 16, 7181 (2008).

[8] R. Liu, Q. Cheng, T. Hand, J. J. Mock, T. J. Cui, S. A. Cummer, and D. R. Smith, "Experimental Demonstration of Electromagnetic Tunneling Through an Epsilon-Near-Zero Metamaterial at Microwave Frequencies", Phys. Rev. Lett. 100, 023903 (2008).

[9] H.-T. Chen, J. F. O'Hara, A. J. Taylor, R. D. Averitt, C. Highstrete, M. Lee, and W. J. Padilla, "Complementary planar terahertz metamaterials," Opt. Express 15, 1084-1095 (2007).

[10] J. Valentine, S. Zhang, T. Zentgraf, E. Ulin-Avila, D. A. Genov, G. Bartal & X. Zhang, "Three-dimensional optical metamaterial with a negative refractive index", Nature| 455, 376 (2008).

[11] A. F. Hoffman et. al., „Negative refraction in semiconductor metamaterials", Nature Materials 6, 946 (2007).

[12] Y. A. Urzhumov and G. Shvets, "Optical magnetism and negative refraction in plasmonic metamaterials", Solid State Comm. 146, 208 (2008).

[13] R. Merlin, "Metamaterials and the Landau–Lifshitz permeability argument: Large permittivity begets high-frequency magnetism", PNAS 106, 1693-1698 (2009).

[14] G. Shvets and Ya. A. Urzhumov, "Engineering Electromagnetic Properties of Periodic Nanostructures Using Electrostatic Resonances", Phys. Rev. Lett. 93, 243902 (2004).

[15] M. Davanco, Y. Urzhumov, and G. Shvets, "The complex Bloch bands of a 2D plasmonic crystal displaying isotropic negative refraction", Opt. Exp. 15, 9681 (2007).

[16] Y. A. Urzhumov, G. Shvets, J. Fan, F. Capasso, D. Brandl, and P. Nordlander, "Plasmonic nanoclusters: a path towards negative-index metafluids", Opt. Exp. 15, 14121 (2007).

[17] V. Lomakin, Y. Fainman, Y. Urzhumov, and G. Shvets, "Doubly negative metamaterials in the near infrared and visible regimes based on thin film nanocomposites", Opt. Exp. 14, 11164 (2006).

[18] X. Zhang, M. Davanco, Y. Urzhumov, G. Shvets, and S. R. Forrest, "From Scattering Parameters to Snell's Law: A Subwavelength Near-Infrared Negative-Index Metamaterial", Phys. Rev. Lett. 101, 267401 (2008).

[19] T. Taubner, D. Korobkin, Y. Urzhumov, G. Shvets, and R. Hillenbrand, "Near-field microscopy through a SiC superlens", Science 313, 1595 (2006).

[20] Yoav Avitzour, Yaroslav A. Urzhumov, and Gennady Shvets, "Wide-angle infrared absorber based on a negative-index plasmonic metamaterial", Phys. Rev. B 79, 045131 (2009).

[21] J. B. Pendry, "Negative Refraction Makes a Perfect Lens", Phys. Rev. Lett. 85 (2000) 3966.

[22] Zubin Jacob, Leonid V. Alekseyev and Evgenii Narimanov, "Optical Hyperlens: Far-field imaging beyond the diffraction limit", Opt. Exp. 14, 8247 (2006).

[23] A. Salandrino and N. Engheta, "Far-field subdiffraction optical microscopy using metamaterial crystals: Theory and simulations," Phys. Rev. B 74, 075103 (2006).

[24] A. A. Govyadinov, and V. A. Podolsky, "Material photonic funnels for subdiffraction light compression and propagation", Phys. Rev. B 73, 155108 (2006)

[25] Zhaowei Liu, Hyesog Lee, Yi Xiong, Cheng Sun, Xiang Zhang, "Far-Field Optical Hyperlens Magnifying Sub-Diffraction-Limited Objects", Science 315, 1686 (2007).

[26] G. Shvets, S. Trendafilov, J. B. Pendry, and A. K. Sarychev, PRL 99, 053903 (2007).

[27] Zhaowei Liu, Stephane Durant, Hyesog Lee, Yuri Pikus, Nicolas Fang, Yi Xiong, Cheng Sun, and Xiang Zhang, "Far-Field Optical Superlens" 7, 403 (2007).

[28] R. Merlin, Science 317, 927 (2007).

[29] Yoav Avitzour and Gennady Shvets, "Manipulating Electromagnetic Waves in Magnetized Plasmas: Compression, Frequency Shifting, and Release", Phys. Rev. Lett. 100, 065006 (2008).

[30] Kosmas L. Tsakmakidis, Allan D. Boardman, & Ortwin Hess, " 'Trapped rainbow' storage of light in metamaterials ", Nature 450, 397 (2007).

[31] G. Shvets and J. S. Wurtele, Phys. Rev. Lett. 89, 115003 (2002).

[32] Shuang Zhang, Dentcho A. Genov, Yuan Wang, Ming Liu, and Xiang Zhang, "Plasmon-Induced Transparency in Metamaterials", Phys. Rev. Lett. 101, 047401 (2008).

[33] N. I. Landy, S. Sajuyigbe, J. J. Mock, D. R. Smith, and W. J. Padilla, "Perfect Metamaterial Absorber", PRL 100, 207402 (2008).

[34] Hu Tao, Nathan I. Landy, Christopher M. Bingham, Xin Zhang, Richard D. Averitt, and Willie J. Padilla, "A metamaterial absorber for the terahertz regime: Design, fabrication and characterization", Opt. Exp. 16, 7181 (2008).

[35] T. J. Coutts, Renewable Sustainable Energy Rev. 3, 77 (1999).

[36] Hou-Tong Chen, Willie J. Padilla, Joshua M. O. Zide, Arthur C. Gossard, Antoinette J. Taylor, and Richard D. Averitt, "Active terahertz metamaterial devices", Nature 444, 597 (2006).

[37] Thomas H. Hand and Steven A. Cummer, "Frequency tunable electromagnetic metamaterial using ferroelectric loaded split rings", J. Appl. Phys. 103, 066105 (2008).